Anisotropy in the *ab*-plane optical properties of $Bi_2Sr_2CaCu_2O_8$ single-domain crystals

M. A. Quijada* and D. B. Tanner
Department of Physics, University of Florida, Gainesville, Florida 32611-8440

R. J. Kelley and M. Onellion
Department of Physics, University of Wisconsin, Madison, Wisconsin 53706

H. Berger and G. Margaritondo
Institut de Physique Appliqué, Ecole Polytechnique Fédérale, CH-1015 Lausanne, Switzerland
(Received 17 June 1999)

The *ab*-plane optical properties of the high-temperature superconductor $Bi_2Sr_2CaCu_2O_8$ are anisotropic in both the normal and the superconducting state. Consistent with the orthorhombic structure, the principal axes lie along the *a* and *b* crystallographic axes, nearly 45° from the Cu-O bond direction. In the normal state, analysis of the temperature-dependent optical conductivity suggests a scattering rate for the free carriers that shows *ab* anisotropy in both magnitude and temperature dependence. In the superconducting state, the anisotropy in the oscillator strength of the superfluid response determined from the far-infrared frequency dependence of $\sigma_2(\omega)$ and from a sum-rule analysis leads to a penetration depth λ_D that is larger along the *b* axis than the *a* axis: ($\lambda_L^b > \lambda_L^a$). [S0163-1829(99)01845-7]

I. INTRODUCTION

There have been many publications about the *ab*-plane anisotropy of the optical properties of the high-temperature superconductors.[1] $YBa_2Cu_3O_{7-\delta}$ was the focus of much of this work;[2–9] its Cu-O chains along the *b* axis are considered to be the cause of the anisotropy in the optical conductivity as well as in the dc transport[10] properties. This assignment follows the conventional approach of separating the response into chain and plane components, with the underlying assumption that the quasi-two-dimensional CuO_2 planes are isotropic.[5–8] In this paper we describe a study of the *ab*-plane anisotropy in the optical properties of single-domain crystals of $Bi_2Sr_2CaCu_2O_8$. Unlike $YBa_2Cu_3O_{7-\delta}$, there are no Cu-O chains, making it possible to study the anisotropy of the CuO_2 planes. One issue is the anisotropy of the order parameter in the superconducting state. A second and equally important issue is the anisotropy of the electronic structure in the normal state.

The CuO_2 planes in $Bi_2Sr_2CaCu_2O_8$ are separated by double Bi_2O_2 layers, which are believed to act as a charge reservoir. There is an orthorhombic distortion in the *ab* plane because of weak superlattice modulation along the *b* axis, which is attributed to an incommensurate defect structure in the Bi_2O_2 layers.[1–13] Note that the *a* and *b* axes in this material are along the Bi-O bonds and nearly 45° from the Cu-O bonds. Based on the very small difference in the *a* and *b* bond lengths (≈0.04 Å), one would expect an almost isotropic *ab*-plane conductivity.

In the experiments reported here, we measured the reflectance of $Bi_2Sr_2CaCu_2O_8$ single-domain crystals for light polarized along the two principal axes in the *ab* plane in a frequency range of 80–33 000 cm^{-1} (10 meV–4.1 eV). The reflectance in the far-infrared and mid-infrared regions was measured for temperatures above and below the superconducting transition temperature. The optical conductivity and related optical constants are obtained from a Kramers-Kronig analysis of the reflectance at each temperature. Analysis of the optical conductivity is carried out using one- and two-component models. A discussion of the anisotropy in the superconducting state will be given in the context of these two models. A detailed study of dc transport measurements performed on similar single-domain crystals is reported elsewhere.[14,15]

II. PREVIOUS WORK ON $Bi_2Sr_2CaCu_2O_8$

The first single-crystal reflectance spectra of $Bi_2Sr_2CaCu_2O_8$ were reported by Reedyk *et al.*[16] The temperature dependence of samples with $T_c = 85$ K was measured in the far infrared and the optical conductivity determined by Kramers-Kronig analysis. Similar spectra were found by other workers.[17–29] The reflectance drops steadily throughout the infrared to a minimum around 10 000 cm^{-1} (1.3 eV). Very little temperature dependence is observed above 1000 cm^{-1}. Also visible are a band centered around 16 000 cm^{-1} (2 eV) as well as structure (with considerable sample-to-sample variation) spanning 28 000–32 000 cm^{-1} (3.5–4 eV). The lower band is interpreted as the Cu-O charge transfer band, while the upper one is most likely associated with excitations of the Bi-O layers.

As first shown by Forro *et al.*,[30] the micaceous nature of the bismuthates makes it possible to prepare thin free-standing flakes of $Bi_2Sr_2CaCu_2O_8$ that are as little as 1000 Å thick and to make infrared transmission studies of these flakes. Because the samples are free standing, the transmittance may be measured over a wide frequency range without interference from a substrate. Romero *et al.*[31] measured the transmittance $\mathcal{T}$ between 80 and 30 000 cm^{-1} at temperatures between 20 and 300 K. The transmittance is low overall, and increases with increasing frequency. The low-frequency $\mathcal{T}$ was rather different above and below the superconducting

transition, with a finite intercept for $T > T_c$ contrasting with $\mathcal{T} \propto \omega^2$ for $T < T_c$. At higher frequencies, $\mathcal{T}$ increases quasilinearly with ω out to ~ 2200 cm^{-1} (0.27 eV); above which it increases more quickly. There is a transmission maximum at 14 000 cm^{-1} (1.8 eV) and a second maximum at 25 000 cm^{-1} (3.1 eV). The linear increase is different from the $\sim \omega^2$ behavior that is expected for a simple metal.[32]

That the *ab* plane itself is not isotropic was observed by Romero and co-workers.[31,33] This anisotropy occurs in spite of the pseudotetragonal crystal structure of this material and the absence of chains. The optical conductivity and other optical constants of $Bi_2Sr_2CaCu_2O_8$ have been estimated by many workers with qualitatively similar results. Reedyk *et al.*,[16] Quijada *et al.*,[24] Puchkov and co-workers,[25,27] Basov *et al.*,[26] and Liu and co-workers[28,29] reported the results of Kramers-Kronig analysis of reflectance. Romero and co-workers[33–35] determined the optical conductivity by Kramers-Kronig analysis of the transmittance. In the normal state the low-frequency conductivity approaches the dc conductivity and falls with increasing frequency. However, above ~ 300 cm^{-1} the decrease in $\sigma_1(\omega)$ is closer to ω^{-1} than the ω^{-2} behavior expected for free carriers. Furthermore, the T dependence of $\sigma_1(\omega)$ at high frequencies is much smaller than at dc or low frequencies. Thus, $Bi_2Sr_2CaCu_2O_8$ displays the non-Drude conductivity that is a common feature of the high-T_c superconductors. Below T_c, $\sigma_1(\omega)$ has a broad maximum around 1000 cm^{-1} (0.15 eV), with some structure in the phonon region. A slight dip in $\sigma_1(\omega)$ can be seen around 400 cm^{-1} (50 meV) although this antiresonance or ''notch'' is not as noticeable as in the $YBa_2Cu_3O_{7-\delta}$ system.

Recently, considerable work has been reported on $Bi_2Sr_2CaCu_2O_8$ samples in the underdoped portion of the phase diagram.[25–27,29] These measurements are in the regime where a pseudogap may occur in the normal state. The pseudogap is not evident in the optical conductivity measured in the *ab* plane. Instead, there is structure in the scattering rate, $1/\tau(\omega,T)$, as calculated from a memory-function analysis of the optical conductivity. In optimally doped materials, the scattering rate is a nearly linear function of the frequency. In contrast, the underdoped cuprates have a scattering rate that is depressed at frequencies below about 700 cm^{-1} at temperatures a little above T_c.

III. EXPERIMENTAL TECHNIQUES AND DATA ANALYSIS

A. Crystal growth and characterization

The $Bi_2Sr_2CaCu_2O_8$ crystals used in the study were grown by using standard techniques as reported elsewhere.[36] In a typical experiment, the starting materials, Bi_2O_3, $SrCO_3$, $CaCO_3$, and CuO are ground and placed in an alumina crucible. The mixture is then heated to a temperature of 50–70 °C above the liquidus temperature and equilibrated for 6 h. The temperature is subsequently lowered to 875–880 °C, and after reaching equilibrium for 6 h, the temperature is slowly cooled at 0.5–2 °C/h to 820 °C, after which the furnace is cooled more quickly. Samples are subsequently annealed in dry oxygen at 600 °C for 8 h and later reannealed in argon at 750 °C for a period of 12 h. This procedure produces samples that are very slightly on the underdoped side of the $Bi_2Sr_2CaCu_2O_8$ phase diagram.

Typical crystals are thin platelets with dimensions of a few millimeters in the *ab* plane. Identification of the *a* and *b* axes was done by using low-energy electron diffraction techniques. The incommensurate superlattice modulation pattern was seen along the *b* axis and not in the perpendicular direction (*a* axis), suggesting the samples were single-domain crystals. The alignment of the principal axes in the crystal was confirmed by observing the extinction points when the sample was rotated under a microscope (Olympus, model BHM) with crossed polarizers. Meissner effect measurements indicate the samples are single phase with the onset of superconductivity around 86 K. This is in good agreement with the onset of superconductivity as determined by using four-probe resistance measurements.[14]

B. Optical techniques

Normal-incidence reflectance of the samples was measured by using a modified Perkin-Elmer 16U grating spectrometer in the near-infrared and ultraviolet regions (2000–33 000 cm^{-1}). The far-infrared and midinfrared regions were covered using a Bruker IFS-113v Fourier transform spectrometer (80–4000 cm^{-1}). Linear polarization of the light was achieved by placing a polarizer of the appropriate frequency range in the path of the beam using a gear mechanism that allowed *in situ* rotation. This setup allowed for very accurate determination of the anisotropy in the reflectance.

Low-temperature measurements (10–300 K) were done by attaching the sample holder assembly to the tip of a continuous-flow cryostat. A flexible transfer line delivered liquid helium from a storage tank to the cryostat. The temperature of the sample was stabilized by using a temperature controller connected to a previously calibrated Si diode sensor and a heating element attached to the tip of the cryostat.

The data acquisition process consisted of measuring spectra at each temperature for both the sample and for a reference Al mirror, and then dividing the sample spectrum by the reference spectrum in order to obtain a preliminary reflectance of the sample. After measuring the temperature dependence in this preliminary reflectance for each polarization, the proper normalizing of the reflectance was obtained by taking a final room-temperature spectrum, coating the sample with a 2000-Å-thick film of Al, and remeasuring this coated surface. A properly normalized room-temperature reflectance was then obtained after the reflectance of the uncoated sample was divided by the reflectance of the coated surface and the ratio multiplied by the known reflectance of Al. This result was then used to correct the reflectance data measured at other temperatures by comparing the individual room-temperature spectra taken in the two separate runs. This procedure corrects for any misalignment between the sample and the mirror used as a temporary reference before the sample was coated and, more importantly, it provides a reference surface of the same size and profile as the actual sample area.

The uncertainties in the absolute value of the reflectance reported here are in the order of $\pm 1\%$, while the uncertainty in the relative anisotropy is much smaller, $\pm 0.25\%$. This

uncertainty is in good agreement with the reproducibility found from the measurements of three different samples.[24]

C. Kramers-Kronig analysis

We estimated the optical constants by Kramers-Kronig transformation of the reflectance data.[37] The low- and high-frequency extrapolations were done in the following way. The conventional low-frequency extrapolation for metals is the so-called Hagen-Rubens relation, $\mathcal{R}(\omega)=1-A\sqrt{\omega}$, where A is a constant determined by the reflectance of the lowest frequency measured in the experiment. For high-T_c samples, this procedure is inadequate; it can only be used as a first approximation. A better procedure extends the low-frequency data using a Lorentz-Drude model, dominated at the low frequencies by the free-carrier (Drude) form. Finite-frequency excitations are modeled by Lorentz oscillators. The fitted reflectance is then used as an extension below the lowest measured frequency. In the superconducting state, the reflectance is expected to be unity for frequencies close to zero. An empirical formula that represents the way $\mathcal{R}$ approaches unity is $\mathcal{R}=1-B\omega^4$, where B is a constant determined from the lowest frequency measured. However, it is better to use the same Lorentz-Drude model, but with the Drude scattering rate set to zero.

At high frequencies, the *ab*-plane anisotropy in the reflectance is consistent with the anisotropy obtained using ellipsometric technique in the visible and UV ranges.[38] We therefore extended the data up to 50 000 cm^{-1} by appending the results of Kelly *et al.*[38] Above this frequency, the reflectance for higher interband transitions was modeled using the formula

$$\mathcal{R}(\omega)=\mathcal{R}_f\left(\frac{\omega_f}{\omega}\right)^s, \tag{1}$$

where $\mathcal{R}_f$ and ω_f are the reflectance and frequency of the last data point. The exponent s is a number that can take up values between 0 and 4; we used $s\sim 2$. At very high frequencies ($\omega_{f'}$), where the free-electron behavior sets in, the approximation used is

$$\mathcal{R}(\omega)=\mathcal{R}_{f'}\left(\frac{\omega_{f'}}{\omega}\right)^4, \tag{2}$$

with $\omega_{f'}$ chosen to be $\sim$100 eV and $\mathcal{R}_{f'}$ adjusted to match smoothly to $\mathcal{R}(\omega)$ from Eq. (1). We observed some dependence of the results for frequencies close to the highest frequencies on the choice of s and $\omega_{f'}$. For lower frequencies, however, the effects due to the choice of the exponent s and $\omega_{f'}$ were insignificant.

IV. THE REFLECTANCE

A. Room-temperature spectra

Figure 1 displays the room-temperature reflectance of $Bi_2Sr_2CaCu_2O_8$ over a wide frequency range for polarization along the *a* and *b* axes. At low frequencies the *a* axis reflectance is 1–2 % higher than the *b* axis reflectance. As the frequency increases, the reflectance in both polarizations falls off in a quasilinear fashion. Near the plasmon minimum, we observe that the plasma edge for the polarization

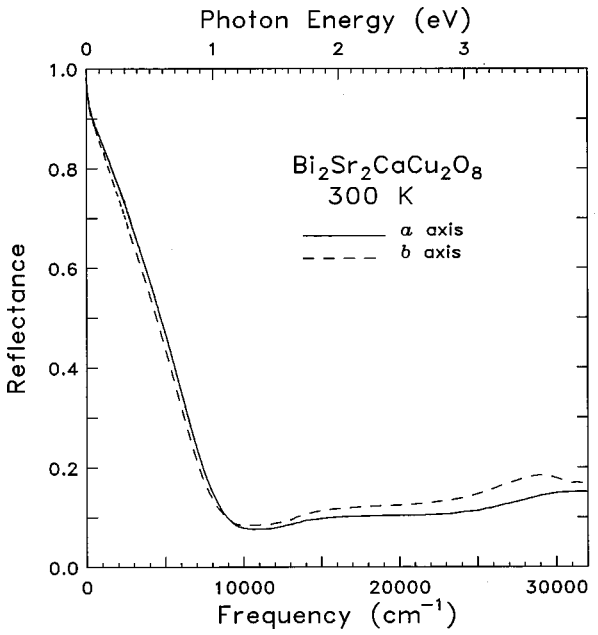

FIG. 1. The 300-K reflectance of $Bi_2Sr_2CaCu_2O_8$ for light polarized along the *a* and *b* axes.

parallel to the *b* axis occurs at a slightly lower frequency than for the *a* axis. The splitting is about 500 cm^{-1}, making the in-plane anisotropy of $Bi_2Sr_2CaCu_2O_8$ much less pronounced than in $YBa_2Cu_3O_{7-\delta}$, where the splitting is about 5500 cm^{-1}. The larger plasma edge along the *b* direction in $YBa_2Cu_3O_{7-\delta}$ has been attributed[2,3,5,8] to the presence of CuO chains along the *b* axis. The anisotropy of $Bi_2Sr_2CaCu_2O_8$, which does not have chains, demonstrates that the electronic structure of the CuO_2 planes is themselves anisotropic. This anisotropy is of course consistent with the orthorhombic structure of $Bi_2Sr_2CaCu_2O_8$. However, the structural anisotropy of the CuO_2 plane is much smaller in $Bi_2Sr_2CaCu_2O_8$ than in $YBa_2Cu_3O_{7-\delta}$. Indeed, because the Cu-O bonds are nearly 45° from the *a* and *b* axes, there is almost no difference in their lengths. $Bi_2Sr_2CaCu_2O_8$ is thus of particular interest because the orthorhombic distortion of the CuO_2 layers appears to be the only reason for the in-plane anisotropy in the optical properties.

At frequencies above the plasmon minimum the reflectance is substantially higher for $\mathbf{E}\|b$. Two interband transitions are evident in this region. The first interband peak is present in both directions, while the second one, centered at 3.8 eV, is more pronounced for the polarization along *b* and is almost absent along the *a* direction. The first peak, at 2.3 eV, is assigned to the charge transfer band of the CuO_2 planes of this material, whereas the second one is most likely associated with interband transitions occurring in the Bi_2O_2 layers. This result is in agreement with ellipsometric measurements of Kelly *et al.*[38]

B. Temperature-dependent spectra

The temperature dependence of the polarized reflectance in the far-infrared and mid-infrared regions is shown in Fig. 2. Two things should be noticed about these data. First, there

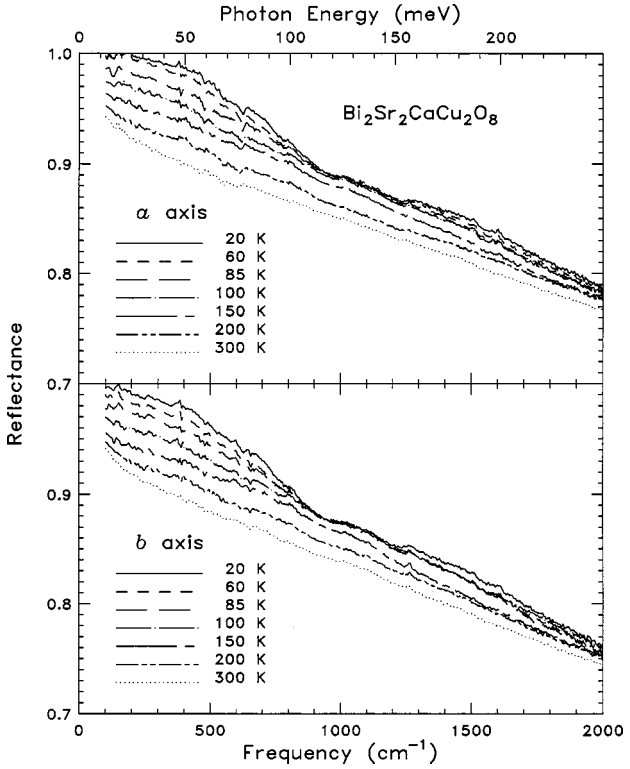

FIG. 2. Temperature dependence of the *a*- and *b*-axis reflectance of $Bi_2Sr_2CaCu_2O_8$.

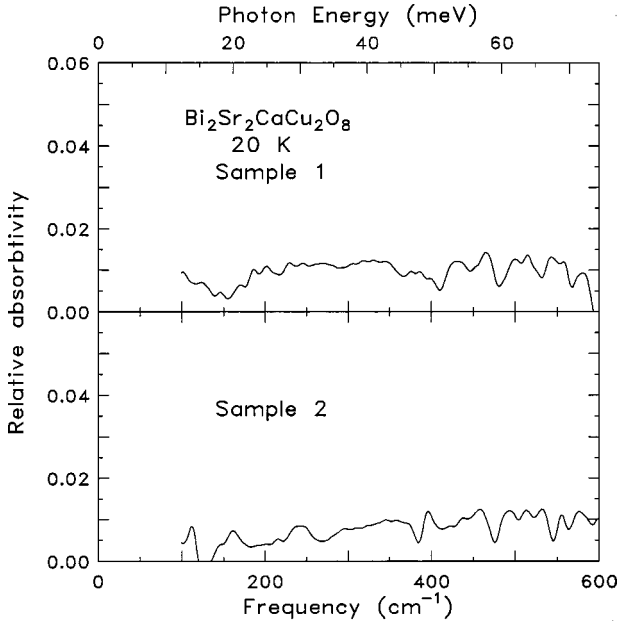

FIG. 3. Relative absorptivity ($\mathcal{R}_a-\mathcal{R}_b=A_b-A_a$) for two different samples in the superconducting state.

is an increase in the far-infrared reflectance as the temperature of the sample is lowered, with two shoulderlike features developing in both polarizations as the sample enters the superconducting state. The first feature is at a frequency between 100 and 200 cm^{-1}; it is followed by a stronger feature at $\omega=400-450\,cm^{-1}$ and a weak minimum around 900 cm^{-1}. The interpretation of these features will be given when discussing the optical conductivity obtained from the Kramers-Kronig analysis.

Second, the reflectance is higher for $\mathbf{E}\|a$ at all frequencies and temperatures. Even when the sample is superconducting, there remains a difference in the reflectance ($\mathcal{R}_a>\mathcal{R}_b$) of about 1%. Romero *et al.*[31] found the transmittance of free-standing single crystals of $Bi_2Sr_2CaCu_2O_8$ to be higher for light polarized along the *a* axis, implying more absorption for the *b*-axis polarization. The reflectance data in Fig. 2 agree with these results.

Figure 3 shows for two different samples the anisotropy in the superconducting-state absorption (at 20 K), defined as $\mathcal{R}_a-\mathcal{R}_b=A_b-A_a$, where $A=1-\mathcal{R}$. In both cases, the low-frequency absorption anisotropy is about 0.5–1 %. Although the accuracy in absolute reflectance is only $\pm1\%$, so that we cannot determine whether the *a*-axis reflectance is indeed unity below 200 cm^{-1}, our accuracy in anisotropy determination is $\pm0.25\%$. This measure of the uncertainty in the anisotropy determination was obtained in two ways. It represents the statistical variation in repeated measures of a single sample; it also represents the reproducibility found from the measurements of three different samples.[24] Therefore, we can say with certainty that the *b*-axis reflectance is *less* than 100% down to $\sim150\ cm^{-1}$ (~20 meV).

V. OPTICAL CONSTANTS

A. Room temperature

The 300-K optical conductivities σ_a and σ_b are shown in Fig. 4. The inset shows the low-energy region on an expanded scale. All of the aspects of the reflectance are also evident here. First, there is a weak anisotropy in the far-infrared conductivity ($\sigma_a>\sigma_b$) that is in agreement with the dc value for similar samples.[14] Second, the low-frequency $\sigma_1(\omega)$ falls off much more slowly than the ω^{-2} dependence of a simple Drude spectrum.[1] For these samples the slope of $\sigma_1(\omega)$ between 400–8000 cm^{-1} region is $\omega^{-0.56\pm0.02}$ for both *a* and *b* directions. This slope is nearly the same as for the *a*-axis room-temperature conductivity[15] of $YBa_2Cu_3O_{7-\delta}$ ($\omega^{-0.53\pm0.02}$). Interpretation of this non-Drude behavior of the optical conductivity of the copper-oxide superconductors has been one of the most debated issues related to the optical properties of these materials.

The upper panel of Fig. 5 shows the energy-loss function, $-\mathrm{Im}(1/\epsilon)$. There is a slight difference in the position of the loss function maxima for the two polarizations. In simple metals, the position of this peak gives the ''screened'' plasma frequency $\widetilde{\omega_p}=\omega_p/\sqrt{\epsilon_\infty}$ and its width is a measure of the scattering rate of the free carriers. However, because of the unusual behavior of the conductivity in the midinfrared, it is difficult to make the same assignment here, unless some assumptions are made about this midinfrared absorption. If a generalized Drude model[39] is used to describe the data, the results lead to a renormalized scattering rate $1/\tau^*$ and an effective mass enhancement m^* for the quasiparticles. The extra absorption is then a consequence of a linear increase of $1/\tau^*$ as the frequency of the light is increased, and the width of the loss function is the value of $1/\tau^*$ at the screened plasma frequency. However, if two or more types of carriers contribute, then the broadening in $-\mathrm{Im}(1/\epsilon)$ is due to the combination of the free Drude-like carriers with other type of bound-carrier excitations in the midinfrared.

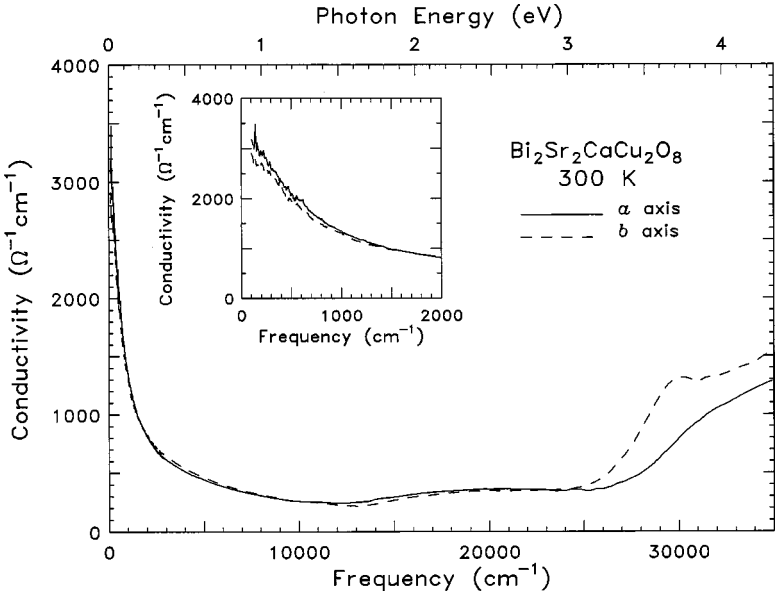

FIG. 4. Room-temperature conductivity on a wide frequency scale for polarization along the principal axes in the *ab* plane of $Bi_2Sr_2CaCu_2O_8$. The inset shows the details of the low-frequency region.

It has been suggested by Bozovic *et al.*[40] that there is a universal frequency dependence in the loss function of all the copper-oxide superconductors, with $-\mathrm{Im}(1/\epsilon)\propto\omega^2$ for small ω. The low-frequency data for $-\mathrm{Im}(1/\epsilon)$ are shown on a log-log scale in the inset of Fig. 5. This plot shows that there are actually two regimes to consider in the $Bi_2Sr_2CaCu_2O_8$ samples we measured. For frequencies below 1000 cm^{-1}, the power-law dependence in $-\mathrm{Im}(1/\epsilon)$ is $\omega^{0.99\pm0.02}$. Only for $\omega>1000\,\mathrm{cm}^{-1}$ does the exponent in ω become on the order of 2. Similar observations were made by Gao *et al.*[41] from measurements on the $La_{2-x}Sr_xCuO_4$ system.

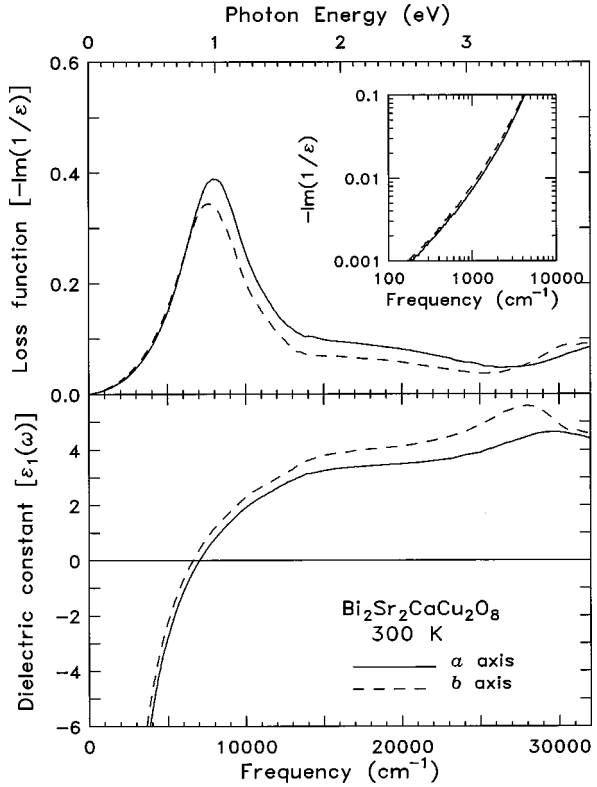

FIG. 5. (Upper panel) Room-temperature loss function $[-\mathrm{Im}(1/\epsilon)]$ on a wide-frequency scale along the principal axes in the *ab* plane of $Bi_2Sr_2CaCu_2O_8$. Inset: Logarithmic scale to show power-law dependence at low frequencies. (Lower panel) real part of dielectric function for the *ab* plane of $Bi_2Sr_2CaCu_2O_8$.

The real part of the dielectric function $\epsilon_1(\omega)$ is shown in the lower panel of Fig. 5. The zero crossing of $\epsilon_1(\omega)$, which also is related to the screened plasma frequency $\widetilde{\omega_p}$, evidently occurs at a lower energy for $\mathbf{E}\|b$ than for $\mathbf{E}\|a$. This difference could be due to either a larger bare plasma frequency ω_p for the charge carriers moving along the *a* direction or to a larger high-frequency dielectric constant ϵ_∞ for $\mathbf{E}\|b$. The more pronounced peak in the interband transition centered at $\omega=3.8$ eV for $\mathbf{E}\|b$ suggests a larger ϵ_∞ for this direction, making the latter the more likely possibility.

Figure 6 shows the results of evaluating the partial sum rule for $\sigma_1(\omega)$. This function is given by

$$N_{\mathrm{eff}}(\omega)\frac{m}{m_b}=\frac{2mV_{\mathrm{cell}}}{\pi e^2}\int_0^{\omega}\sigma(\omega')d\omega', \tag{3}$$

where e and m are the free-electron charge and mass, respectively, m_b the effective mass, and V_{cell} the volume occupied by one formula unit of $Bi_2Sr_2CaCu_2O_8$. The curves give the effective number of carriers per formula unit participating in optical transitions below frequency ω. Although N_{eff} is roughly isotropic at low frequencies, some differences appear at higher energies, particularly in the interband region where transitions in the Bi_2O_2 layers are thought to occur.[38] At a frequency of 12 000 cm^{-1} (1.5 eV), the onset of the charge-transfer band, $N_{\mathrm{eff}}\approx0.75$. Thus, assuming an effective mass of $m_b=m$, there are about 0.37 carriers per CuO_2 unit.

B. Temperature dependence of the optical conductivity

The temperature evolution of the optical conductivity is shown in Figs. 7(a) and 7(b) for $\mathbf{E}\|a$ and $\mathbf{E}\|b$, respectively. There are several important features to these spectra. First, in the normal state (100–300 K) the low-frequency optical conductivity extrapolates reasonably well to the dc conductivity. For example, at 300 K the *a*-axis conductivity extrapolates to about 3400 Ω^{-1} cm^{-1}; the *b*-axis to about 3000 Ω^{-1} cm^{-1}.

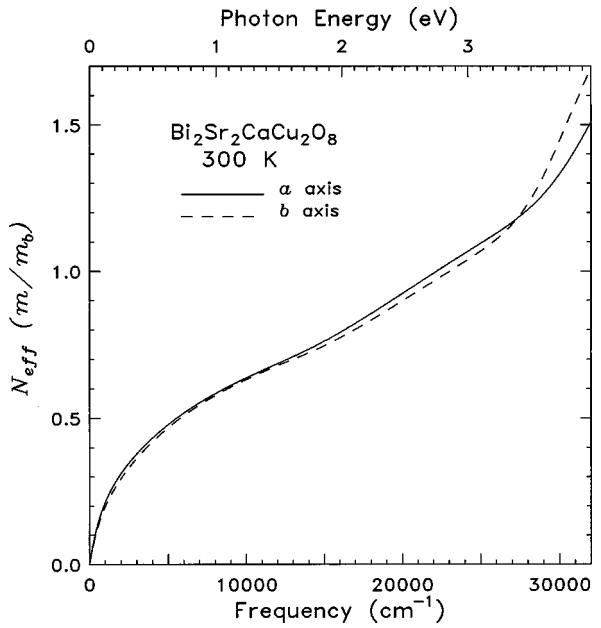

FIG. 6. The results of evaluating the partial sum rule for the room-temperature conductivity of $Bi_2Sr_2CaCu_2O_8$.

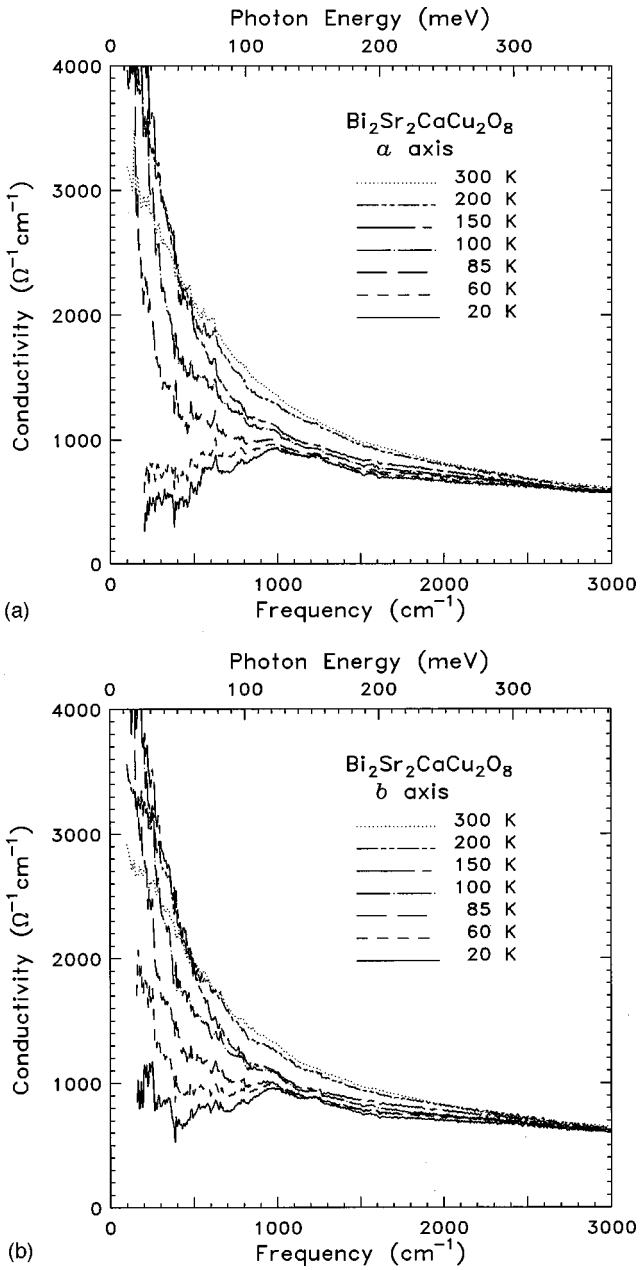

FIG. 7. (a) Temperature dependence of the *a*-axis optical conductivity obtained from Kramers-Kronig analysis of the reflectance. (b) Temperature dependence in the *b*-axis optical conductivity obtained from Kramers-Kronig analysis of the reflectance.

These values correspond to resistivities of 290 and 330 $\mu\Omega$ cm for *a* and *b*, respectively.

Second, with decreasing temperature, the low-frequency conductivity increases strongly, in agreement with the *T*-linear resistivity. There is a characteristic narrowing of this far-infrared portion of the spectrum. This narrowing can be seen most easily by noting that the 300-K data are larger than the lower-temperature data above about 500 cm^{-1} but then crosses through each of the lower temperature curves at progressively lower frequencies, becoming the smallest conductivity near 100 cm^{-1}. Third, at high frequencies, $\sigma_1(\omega)$ does not show much temperature variation; all the curves draw together around 3000 cm^{-1}.

Below T_c, the low-frequency conductivity is considerably reduced, so that the 20-K conductivity is smallest at all frequencies measured. The ''missing area'' in the far-infrared conductivity appears as the zero-frequency delta-function response of the superfluid. This aspect is discussed in more detail below. In addition, a minimum develops around $\omega \approx 400\ cm^{-1}$ in the superconducting state. This feature is visible for both polarizations, but is most evident in the *b*-axis data. The lower reflectance of the *b* polarization is responsible for the upturn observed in $\sigma_1(\omega)$ at the lowest temperature for this polarization. This result may have interesting consequences for the understanding of dynamic properties in these materials. For instance, it indicates the presence of low-lying excitations for carriers moving along the *b* axis that are not present in the perpendicular direction. It is not clear what the origin of these excitations is. Perhaps, the presence of the superlattice structure in the *b* axis may introduce an additional source for scattering along this crystallographic direction. (However, on account of the periodicity of the superlattice, one should not expect any additional scattering process for this direction.)

In some studies, structure in the conductivity around 400 cm^{-1} has been interpreted as evidence of the superconducting energy gap.[3] The fact that we observe the feature for the polarization along *b*, which has reflectance lower than unity, contradicts the conventional (*s*-wave) notion of a gap, where for frequencies below 2Δ no excitations are allowed.

We note that photoemission experiments on samples from the same batch as the ones used in this study have shown evidence for the opening of a gap below T_c in the energy spectrum around the Fermi level.[42,43] The maximum gap parameter obtained from the analysis of the photoemission data has a value of Δ close to 25 meV (at least along the *a* axis). Although twice this energy is close to the minimum position observed in the conductivity data, the minimum in the conductivity cannot be assigned to the superconducting energy gap. Moreover, since similar structures at about this energy are observed in all copper-oxide superconductors, they have

also been explained as due to strong bound-carrier interactions with phonon excitations.[44–47]

VI. APPROACHES TO THE OPTICAL PROPERTIES

In this section, we discuss the normal-state optical conductivity in the far-infrared and mid-infrared regions. This is the frequency range below the charge-transfer gap of the insulating phase of the cuprates; thus, it is the region where the dynamics of the doped-in charge carriers may be studied. Two approaches are used, called ''one-component'' and ''two-component.'' In the first, there is only a single band or type of carrier, and the unusual frequency dependence in the mid-infrared is attributed to interaction with a spectrum of (optically inactive) excitations. This interaction causes a frequency dependence to the carrier scattering rate and enhances the low-frequency effective mass.

In the two-component approach, two different contributions are assumed: the Drude response of free carriers and a second band of ''mid-infrared'' carriers. The properties of the Drude carriers determine the dc conductivity, including its temperature dependence, while the mid-infrared carriers dominate the higher frequency conductivity.

A. One-component analyses

Many authors[3,7,8,25,26] have analyzed $\sigma_1(\omega)$ using a generalized Drude model with a frequency-dependent scattering rate. In this approach, there is only one type of charge carrier. Hence, the dielectric function can be written as[39]

$$\epsilon(\omega)=\epsilon_\infty-\frac{\omega_p^{*2}}{\omega^2+i\omega/\tau^*(\omega)}, \tag{4}$$

where ϵ_∞ is a constant that includes contributions from interband transitions, the plasma frequency $\omega_p^*=(m/m^*)\omega_p$ with m^* the effective mass, and ω_p the bare plasma frequency, defined by $\omega_p=\sqrt{4\pi Ne^2/m_b}$. The quantity $1/\tau^*(\omega)$, known as the ''renormalized'' relaxation rate, may easily be calculated,

$$1/\tau^*=\frac{4\pi\sigma_1(\omega)}{\epsilon_1(\omega)-\epsilon_\infty}, \tag{5}$$

without knowing ω_p.

It is also possible to use a complex relaxation rate, or memory function,[39] $G=1/\tau(\omega)-i\omega\lambda(\omega)$ with $1/\tau(\omega)$ the ''unrenormalized'' carrier scattering rate and $\lambda(\omega)$ the mass enhancement factor. $[m^*=m(1+\lambda).]$ The dielectric function is

$$\epsilon(\omega)=\epsilon_\infty-\frac{\omega_p^2}{\omega^2[1+\lambda(\omega)]+i\omega/\tau(\omega)}. \tag{6}$$

In this memory-function approach the relaxation rate may be calculated from

$$1/\tau(\omega)=-\frac{\omega_p^2}{\omega}\mathrm{Im}\left(\frac{1}{\epsilon(\omega)-\epsilon_\infty}\right). \tag{7}$$

Models providing a phenomenological justification for this approach include the ''marginal Fermi liquid'' (MFL) theory of Varma and co-workers[48,49] the ''nested Fermi liquid'' (NFL) theory of Virosztek and Ruvalds,[50] the ''Luttinger liquid'' picture of Anderson,[51] the proposal that the conductivity is a paraconductivity involving phase separation, advocated by Emery and Kivelson,[52] and the nearly antiferromagnetic Fermi liquid picture of Monthoux and Pines.[53] In many of these the scattering rate is simply given by the temperature.

In the MFL, the imaginary part of the one-particle self-energy is written as

$$-\mathrm{Im}\,\Sigma(\omega)\sim\begin{cases}\pi^2\lambda T, & \omega<T\\ \pi\lambda\omega, & \omega>T,\end{cases} \tag{8}$$

where λ is a dimensionless coupling constant. For $\omega<T$ the model predicts a renormalized scattering rate that is linear in temperature, which is in accord with the linear temperature dependence in the resistivity that is observed in nearly all copper-oxide superconductors. As ω increases a new spectrum of excitations comes into play, causing the scattering rate to grow linearly with frequency up to a cutoff frequency ω_c, which is also included in the model.

The physical source of this behavior is the coupling of the charge carriers to a spectrum of charge and/or spin-density fluctuations. The strong frequency dependence arises from a Holstein[54] process, where an electron can absorb a photon, emit some other excitation, and scatter. Energy conservation requires the photon frequency ω to be greater than the excitation frequency Ω. Thus the scattering by this process turns on at the onset of the excitation spectrum and becomes stronger with increasing frequency until the maximum excitation frequency is reached.

Romero *et al.*[34] analyzed their optical conductivity for $Bi_2Sr_2CaCu_2O_8$ and $Bi_2Sr_2CuO_6$ to obtain Σ, finding $\lambda\approx0.27$ for both materials. The MFL equations for the self-energy agree with the data in several important ways. First, both give a dc resistivity in agreement with experiment. Second, $-\mathrm{Im}\,\Sigma$ increases linearly with ω for $\omega>T$. Third, there is an enhancement of the effective mass at low frequencies by an amount that is larger at lower temperatures.

The dielectric function for the MFL can be written as[48,49]

$$\epsilon(\omega)=\epsilon_\infty-\frac{\omega_p^2}{\omega^2-2\omega\Sigma(\omega/2)}+\sum_{j=1}^{N}\frac{\omega_{pj}^2}{\omega_j^2-\omega^2-i\omega\gamma_j}, \tag{9}$$

where ω_p is the bare plasma frequency for the charge carriers, defined by $\omega_p^2=4\pi ne^2/m_b$ with n the carrier density and m_b the band mass of the carriers. The quantity $\Sigma(\omega)$ represents the quasiparticle self-energy. The real part of Σ is related to the effective mass m^* of the interacting carriers by[49] $m^*(\omega)/m_b=1-2\,\mathrm{Re}\,\Sigma(\omega/2)/\omega$, whereas the imaginary part is related to the quasiparticle lifetime through $1/\tau^*(\omega)=-2m_b\,\mathrm{Im}\,\Sigma(\omega/2)/m^*(\omega)$. The factors of 2 arise because quasiparticle excitations come in pairs. The second term is a sum of Lorentzian oscillators (of strength ω_{pj}, center frequency ω_j, and width γ_j) representing contributions from interband transitions. The remaining term, ϵ_∞, is the contribution from transitions above the highest measured frequency.

Figure 8 shows the result of fitting Eq. (9) to our data for the *a*-axis conductivity. The data are shown as heavy dashed lines whereas the fits are shown as thin solid lines. The con-

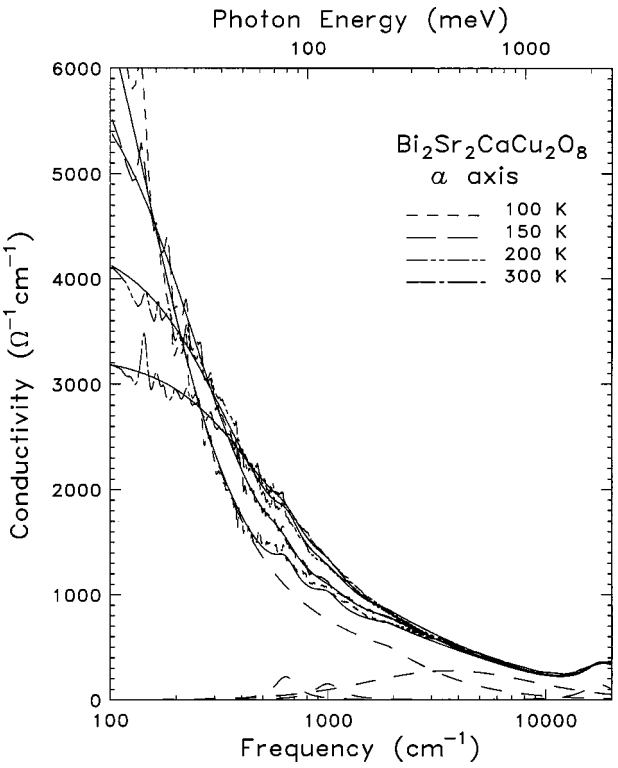

FIG. 8. Fits to the *a*-axis conductivity using the marginal Fermi liquid (MFL) model. The fit is the thin solid line; components of the fit (MFL conductivity, two weak ~100-meV bands, a 0.5-eV band, and the 2-eV charge-transfer band) are thin dashed lines.

ductivities of the MFL contribution for $T=100\,\mathrm{K}$ and the first four Lorentzian lines are shown as thin dashed lines. (The last of these represents the charge-transfer band of the insulating parent compound.) The Lorentzian contributions are small for frequencies below the MFL cutoff frequency $\omega_c \approx 1800\,\mathrm{cm}^{-1}$; they contain less than 2% of the low-energy spectral weight. The third band, however, at 3600 cm^{-1}, is nearly as strong as the MFL contribution. Similar results were obtained for the *b* axis, and the parameters for both principal axes are listed in Table I. Interestingly both the plasma frequency and the coupling constant λ are larger for the *b* polarization than for the *a* polarization. The analysis of Romero and co-workers[34] for unpolarized data gave results midway between these.

As an alternative to fitting, the scattering rate and effective mass functions may be calculated from Eq. (4) once good estimates for ϵ_∞ and ω_p are obtained. Figure 9 shows m^*/m_b and $1/\tau^*(\omega)$ at room temperature for $Bi_2Sr_2CaCu_2O_8$ along the *a* and *b* axes. The values used were $\omega_{pa}=16\,200\,\mathrm{cm}^{-1}$ and $\epsilon_{\infty a}=4.6$; $\omega_{pb}=16\,240\,\mathrm{cm}^{-1}$ and $\epsilon_{\infty b}=4.8$. In Fig. 9 it is interesting to notice that the mass enhancement at low frequencies is isotropic in the *ab* plane, on account of the nearly isotropic values of ω_p. In contrast, Fig. 9 shows an anisotropic renormalized scattering rate that increases linearly with frequency. The linear increase is in agreement with the predicted behavior in the MFL and NFL models.

The temperature dependence of the unrenormalized scattering rate is shown Fig. 10. The upper panel shows $1/\tau$ at five temperatures for the *a* direction and the lower panel shows the same thing for the *b* direction. We note that these functions are not so linear as $1/\tau^*$. The basic behavior, with the low-frequency values increasing with increasing temperature and the high-frequency parts nearly temperature independent, is in accord with the ideas of the MFL and NFL models.

B. The pseudogap

Recent one-component analyses of the infrared properties of underdoped $Bi_2Sr_2CaCu_2O_8$ have been used to suggest a pseudogap in the normal state.[25–27] The pseudogap is not evident in the optical conductivity measured in the CuO_2 planes. Instead, there is structure in the $1/\tau(\omega,T)$ in the *ab*-plane, a depressed scattering rate at low frequencies and at

TABLE I. Parameters of MFL model fits (frequencies in cm^{-1}).

		a axis			*b* axis		
	T (K)	ω_p	λ	ω_c	ω_p	λ	ω_c
MFL	100	13 100	0.23	1900	14 050	0.32	1 790
	150	13 500	0.24	1900	14 100	0.30	1 790
	200	13 800	0.26	1750	14 300	0.32	1 800
	300	13 500	0.23	1800	13 700	0.26	1 790
	T (K)	ω_{pj}	ω_j	γ_j	ω_{pj}	ω_j	γ_j
Lorentzian 1	100	1 570	640	190	1 900	640	460
	150	1 690	610	290	1 250	650	300
	200	1 650	650	220	1 760	660	300
	300	1 570	640	280	1 270	650	650
Lorentzian 2	100	1 790	1 000	350	750	1 000	120
	150	1 890	1 030	600	870	1 050	380
	200	2 160	1 000	570	1 330	1 050	380
	300	1 790	1 020	430	1 260	1 050	550
Lorentzian 3	All	12 300	3 650	9200	12 600	3 700	11 000
Charge transfer band	All	7 700	17 500	6800	6 400	17 100	5 800

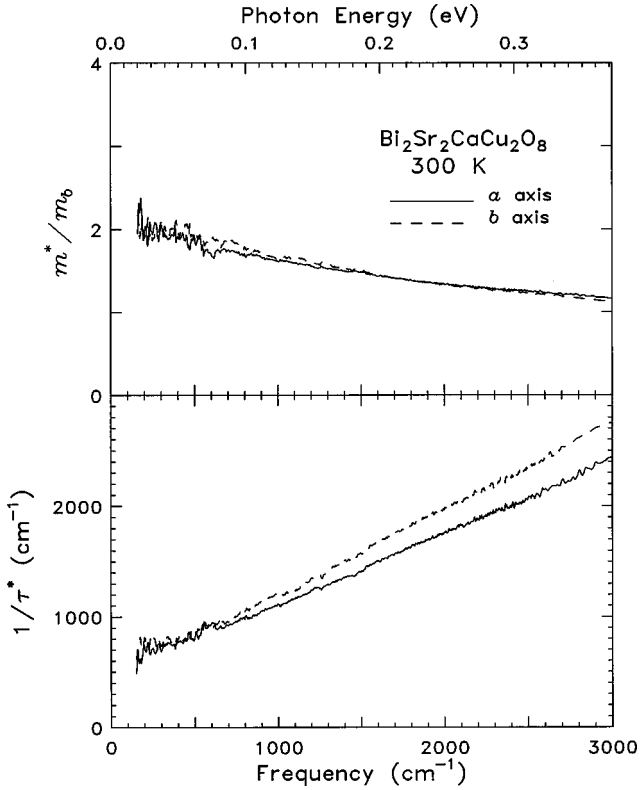

FIG. 9. One-component analysis showing the effective mass enhancement (upper panel) and the renormalized scattering rate (lower panel) along the *a* and *b* axes.

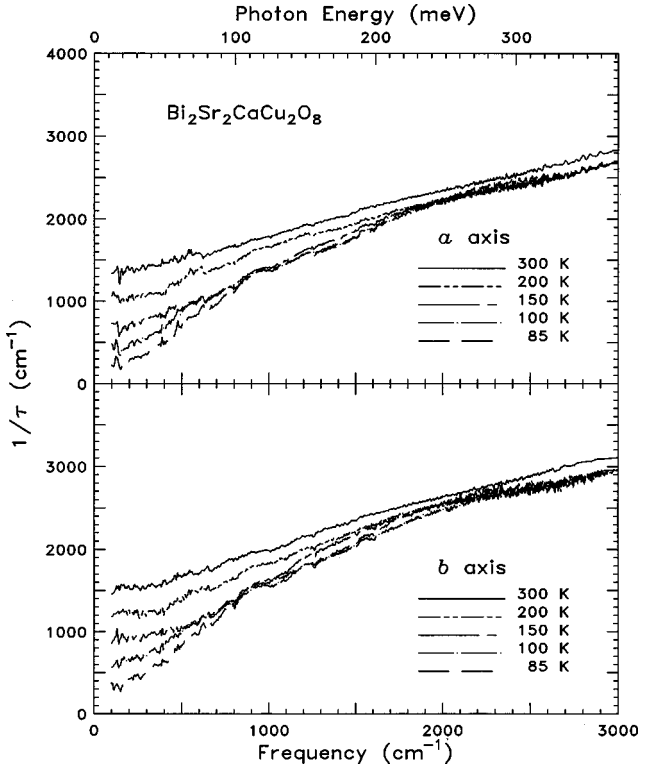

FIG. 10. Temperature dependence of the unrenormalized scattering rate $1/\tau(\omega)$ for the *a* (upper panel) and *b* (lower panel) axes.

temperatures a little above T_c. The scattering rates of Fig. 10 do not show evidence for the pseudogap, suggesting that the materials we have measured are near optimum doping, in agreement with the linear dc resistivity of our crystals.

C. Two-component analysis

Here, we assume that the infrared conductivity is composed of two components. The underlying reason for this analysis is based on two essential observations. First, the optical conductivity $\sigma_1(\omega)$ obtained from doping-dependent studies clearly shows the appearance of freelike as well as bound excitations in the midinfrared as doping in the CuO_2 planes of the samples is increased.[55–60] Second, there is a narrow range of frequencies in the far infrared where $\sigma_1(\omega)$ shows a variation with *T* that is consistent with the *T*-linear resistivity of optimally doped samples. At higher frequencies, $\sigma_1(\omega)$ shows a weaker temperature dependence.[35,41,61–63] The data shown in Fig. 7 exhibit a behavior that is consistent with this observation.

This separation into mid-infrared and free-carrier contributions has been used in several previous studies of $Bi_2Sr_2CaCu_2O_8$. Reedyk *et al.*[16] and Romero *et al.*[34,35] analyzed the optical conductivity of $Bi_2Sr_2CaCu_2O_8$ in this way. The results are similar to the results of Kamarás *et al.*[63] for $YBa_2Cu_3O_{7-\delta}$: there is an apparent onset of mid-infrared conductivity around 100 cm^{-1}, structure in the phonon region, and a broad maximum around 1000 cm^{-1} (0.12 eV). The free-carrier component has a nearly *T*-independent plasma frequency, and a *T*-linear scattering rate. This *T*-linear scattering rate combined with a *T*-independent plasma frequency is, of course, completely consistent with the dc conductivity.

Thus, the dielectric function is assumed to be made up of at least four parts:

$$\epsilon(\omega)=\epsilon_D+\epsilon_{\mathrm{MIR}}+\epsilon_{\mathrm{interband}}+\epsilon_\infty, \tag{10}$$

where ϵ_D is associated with the free-carrier or Drude-like part, ϵ_{MIR} corresponds to the mid-infrared bound transitions, $\epsilon_{\mathrm{interband}}$ includes higher-frequency interband transitions, and ϵ_∞ is the limiting high-frequency value. One way of separating individual contributions uses a Drude-Lorentz model. To describe each component requires three parameters: linewidth γ, plasma frequency ω_p, and center frequency ω_0. The model dielectric function is then

$$\epsilon(\omega)=\epsilon_\infty-\frac{\omega_{pD}^2}{\omega^2+i\omega/\tau}+\sum_j\frac{\omega_{pj}^2}{\omega_j^2-\omega^2-i\omega\gamma_j}, \tag{11}$$

where the second term is the Drude response of the free carriers (ω_{pD} is their plasma frequency and $1/\tau$ is their scattering rate), the sum runs over the midinfrared bands, the charge-transfer band (the band gap of the insulating parent compound), and higher-energy interband transitions. Each band is characterized by a plasma frequency ω_{pj}, center frequency ω_j, and width γ_j.

The results of fitting the reflectance calculated using the dielectric function in Eq. (11) to our data is shown in Fig. 11. The fit, employing two oscillators for the midinfrared region, one for the charge-transfer band, and two for higher-energy interband transitions, is good. To fit the reflectance below T_c we assumed a Drude linewidth of a fraction of a cm^{-1}; i.e.,

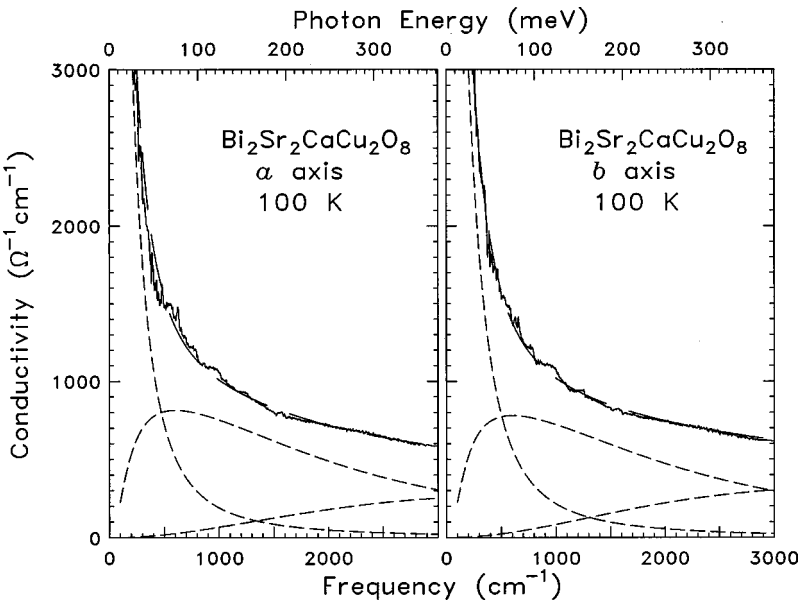

FIG. 11. The *a*- and *b*-axis conductivity at 100 K and fits to a two-component model. The fit is the thin solid line, and the Drude and midinfrared components are the dashed lines.

we collapsed the Drude conductivity to a delta function. The parameters of the fit are listed in Table II. The Drude weight is a little larger for the *a* polarization, as is the strength of the first (~90 meV) mid-infrared band. In contrast, the ~0.5 eV mid-infrared band has more oscillator strength for the *b* polarization.

As an alternative to least-square fitting, a self-consistent approach to separate the Drude-like from the boundlike excitations was used by Romero *et al.*.[34,35] What follows is a brief description of this method applied to the conductivity curves shown in Fig. 7. In the superconducting state and for $T \ll T_c$, all the free-carrier part is presumed to have collapsed into a delta function at $\omega = 0$. Therefore, in first approximation the total conductivity at the lowest temperature ($T = 20$ K) has a negligible free-carrier contribution; it corresponds to the $\sigma_{1\mathrm{MIR}}$ term in Eq. (10). Hence, the free-carrier

TABLE II. Parameters of Drude-Lorentz model fits (frequencies in cm^{-1}).

		a axis			*b* axis		
	T (K)	ω_{pD}		$1/\tau$	ω_{pD}		$1/\tau$
Drude	20	9 250			8 890		
	65	9 180			8 760		
	85	9 200		73	8 800		100
	100	9 040		128	8 750		157
	150	9 080		202	8 740		240
	200	9 100		300	8 770		327
	300	9 020		423	8 700		435
	T (K)	ω_{pj}	ω_j	γ_j	ω_{pj}	ω_j	γ_j
Mid-IR 1	20	10 800	865	2480	10 170	827	2380
	65	10 800	759	2510	10 270	772	2370
	85	10 800	667	2430	10 150	765	2300
	100	11 000	675	2410	10 330	700	2260
	150	10 900	631	2360	10 410	500	2530
	200	10 900	790	2330	10 360	793	2290
	300	10 600	798	2280	10 100	783	2220
Mid-IR 2	20	10 600	4 500	7930	12 310	4 060	8710
	65	10 700	4 320	8030	12 220	3 920	8570
	85	10 500	4 230	7710	12 000	3 960	8420
	100	10 300	4 520	7740	11 880	4 120	8220
	150	10 300	4 430	7660	12 120	3 700	9060
	200	10 300	4 520	7850	12 000	4 060	8660
	300	10 300	4 440	7480	12 000	4 120	8220
Charge transfer band	All	7 700	17 500	6800	6 400	17 100	5800

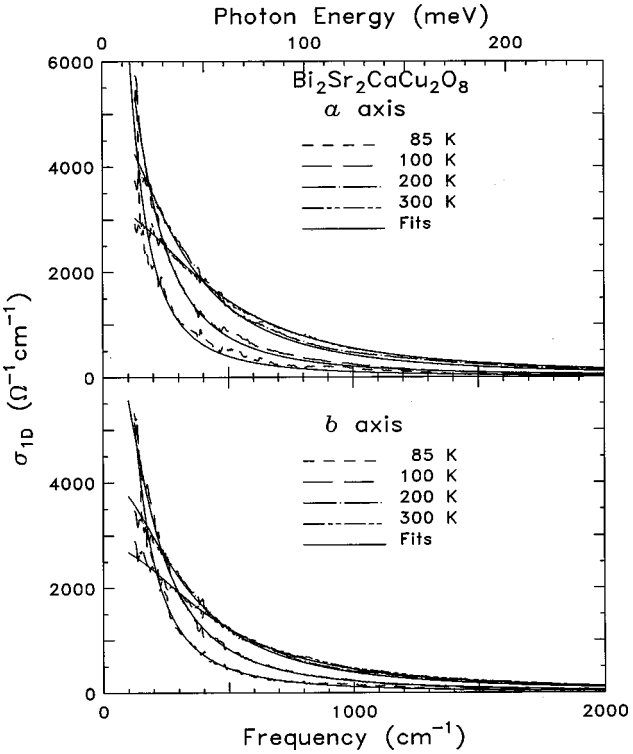

FIG. 12. Drude part from a two-component analysis of $\sigma_1(\omega)$ and fits obtained at each temperature. Top panel, *a* axis; bottom panel, *b* axis.

part in the normal state can be obtained by subtracting $\sigma_{1\mathrm{MIR}}$ from the experimental $\sigma_1(\omega)$ at $T>T_c$.

This first iteration produces free-carrier conductivity ($\sigma_{1D}^{(1)}$) at individual temperatures above T_c. If this conductivity has a Drude line shape, a fit of straight line to the curve obtained by plotting $1/\sigma_{1D}^{(1)}$ vs ω^2 will yield a slope and intercept that can be used to get initial guess values for ω_{pD} and $1/\tau$. Once values for ω_{pD} and $1/\tau$ are obtained, they can be used to calculate a Drude conductivity from

$$\sigma_{1D}^{\mathrm{fit}}=\frac{1}{4\pi}\frac{\omega_{pD}^2\tau}{1+\omega^2\tau^2}. \tag{12}$$

Then, a new mid-infrared conductivity $\sigma_{1\mathrm{MIR}}$ is generated at each temperature by subtracting $\sigma_{1D}^{\mathrm{fit}}$ from the total $\sigma_1(\omega)$ at each temperature above T_c. A self-consistent check of the ω_{pD} and $1/\tau$ obtained at each temperature is done by first computing an average mid-infrared conductivity $\langle\sigma_{1\mathrm{MIR}}\rangle$ from the $\sigma_{1\mathrm{MIR}}$ obtained as explained above, and using this average as the starting mid-infrared term in a second iteration. We found the parameters converge after performing three or four iterations.

1. Drude component

The Drude conductivities $(\sigma_1(\omega)-\langle\sigma_{1\mathrm{MIR}}\rangle)$ obtained from this analysis are shown in Fig. 12 along with fits obtained from the estimates for ω_{pD} and $1/\tau$ at each temperature. The normal-state Drude plasma frequency is nearly temperature independent. We find $\omega_{pD}^a=9300\pm200\,\mathrm{cm}^{-1}$, while $\omega_{pD}^b=8900\pm200\,\mathrm{cm}^{-1}$. Note that these values are a little larger (but within error bars) of the parameters in Table II. The constant plasma frequency means that the oscillator strength and the carrier density do not change with temperature.

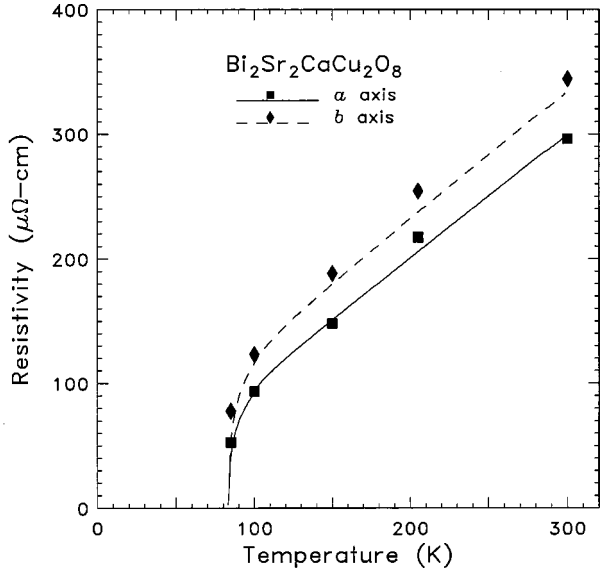

FIG. 13. Temperature dependence of the *a*- and *b*-axis resistivities obtained from dc transport measurements and extrapolations of the optical conductivity.

Figure 13 shows as symbols the Drude resistivity $4\pi/\omega_{pD}^2\tau$ for both polarizations as a function of temperature. The dc resistivity measured for the *a* and *b* axes on similar samples is shown as the full and dashed lines. Two things should be noticed about this figure. The first is that ρ_{dc} and ρ_{optic} both have a linear temperature dependence. Second, there is good agreement between the anisotropy determined from optical and from dc transport measurements.

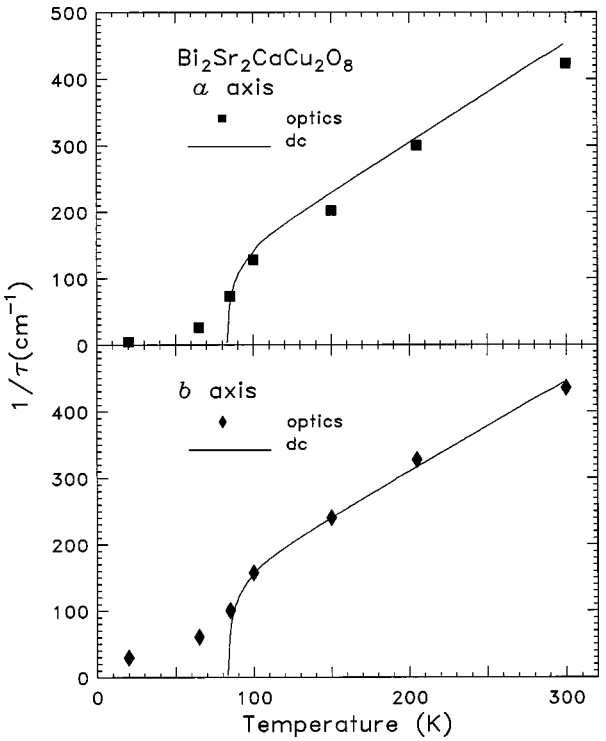

FIG. 14. Scattering rate $(1/\tau)$ obtained from dc transport and the two-component analysis of the optical conductivity.

Figure 14 shows a comparison of $1/\tau_{\rm optic}$ obtained from the fits with $1/\tau_{\rm dc}$ obtained from

$$1/\tau_{\rm dc}=\frac{\omega_{pD}^2}{4\pi}\rho_{\rm dc}, \tag{13}$$

where ω_{pD} is the average Drude oscillator strength. This figure shows that the temperature variation of $1/\tau_{\rm dc}$ and $1/\tau_{\rm optic}$ is indeed linear in the normal state as expected. A linear temperature dependence of $1/\tau$ in metals is a high-temperature phenomenon, with[1,64]

$$\hbar/\tau=2\pi\lambda k_B T+\hbar/\tau_0, \tag{14}$$

where λ is a dimensionless constant that measures the strength of the coupling of the free carriers to whatever excitations are causing the scattering. We find $\lambda_a\sim 0.35$, while $\lambda_b\sim 0.31$. These results are in good agreement with previously estimated values for λ using a two-component analysis in other samples.[1] Furthermore, these results suggest the transport properties of the copper-oxide superconductors are in the weak-coupling regime.

In the superconducting state, $1/\tau_{\rm dc}$ drops to zero on account of $\rho_{\rm dc}$ also going to zero. At the same temperature $1/\tau_{\rm optic}$ also exhibits a sudden drop. This sudden drop suggests that the excitations that cause the scattering of the carriers in the normal state are suppressed below T_c. The limited number of points and possible uncertainties, especially at the lowest frequencies, prevent us from extracting the temperature dependence of $1/\tau$ in the superconducting state. Nonetheless, we do find that the $1/\tau_{\rm optic}$ obtained is larger for the *b* axis than for the *a* axis in the superconducting state. This evidence for an additional channel for elastic scattering in the crystallographic *b* direction is also consistent with the final intercept observed in $\rho_{\rm dc}^b$ from extrapolations to the zero temperature value $\rho_{\rm dc}$.

Sudden drops in the quasiparticle scattering rate as the sample becomes superconducting have been observed in unpolarized infrared measurements of $Bi_2Sr_2CaCu_2O_8$,[35] $La_{2-x}Sr_xCuO_4$,[41] and $YBa_2Cu_3O_{7-\delta}$,[65] and in experiments of femtosecond optical transient and microwave absorption measurements on $YBa_2Cu_3O_{7-\delta}$,[66] and on $(BiO)_2Sr_2Ca_2Cu_3O_{10}$.[67] Similarly, there have been predictions of drop of the quasiparticle scattering rate in the superconducting state within the phenomenology of the marginal Fermi liquid approach.[68] This sudden drop in $1/\tau$ has been proposed as the reason for the appearance of a ''coherence'' peak in $\sigma_1(\omega)$ in studies of $YBa_2Cu_3O_{7-\delta}$ thin films[65,69,70] and in $Bi_2Sr_2CaCu_2O_8$ single crystals[35,71] for temperatures just below T_c and for frequencies in the microwave region.

2. Mid-infrared absorption

The mid-infrared conductivity, that which remains after subtracting the Drude term or low-frequency part, is shown in the top and bottom panels of Fig. 15 for the *a* and *b* axes, respectively. $\sigma_{\rm 1MIR}$ does not have much temperature dependence. Most of the temperature dependence in $\sigma_1(\omega)$ comes from the free-carrier contribution.

To illustrate the anisotropy, Fig. 16 compares $\sigma_{\rm 1MIR}$ for the *a* and *b* directions at 100 and 200 K. The onset of absorption appears around 250 $\rm cm^{-1}$ for the *a* axis, whereas the

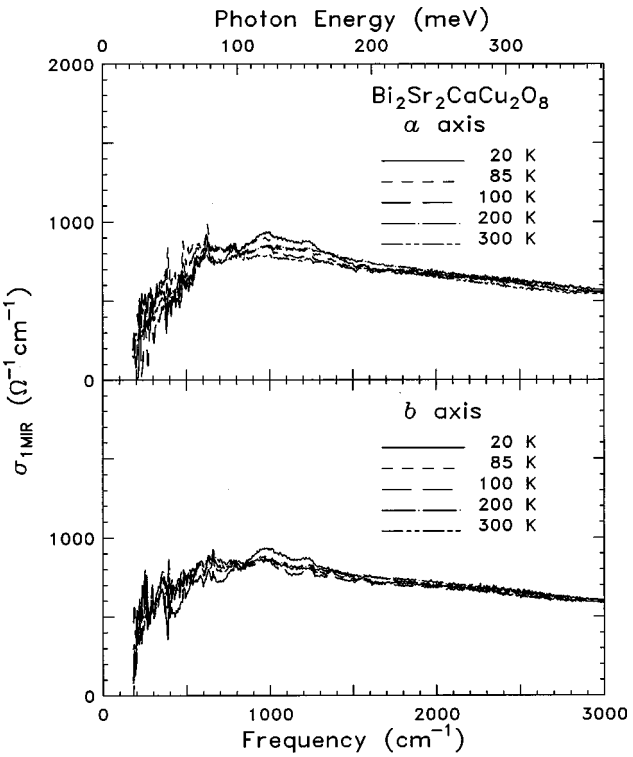

FIG. 15. Mid-infrared part of the total conductivity.

b-axis absorption extends to lower frequencies (150–200 $\rm cm^{-1}$) and is higher in the frequency range 150–700 $\rm cm^{-1}$. In both cases, there is weak structure due to phonons, including weak minima at $\omega\sim 400$ and 800 $\rm cm^{-1}$. Figure 15 shows that these minima appear in both the normal and superconducting states. Earlier optical studies[3,7] interpreted this

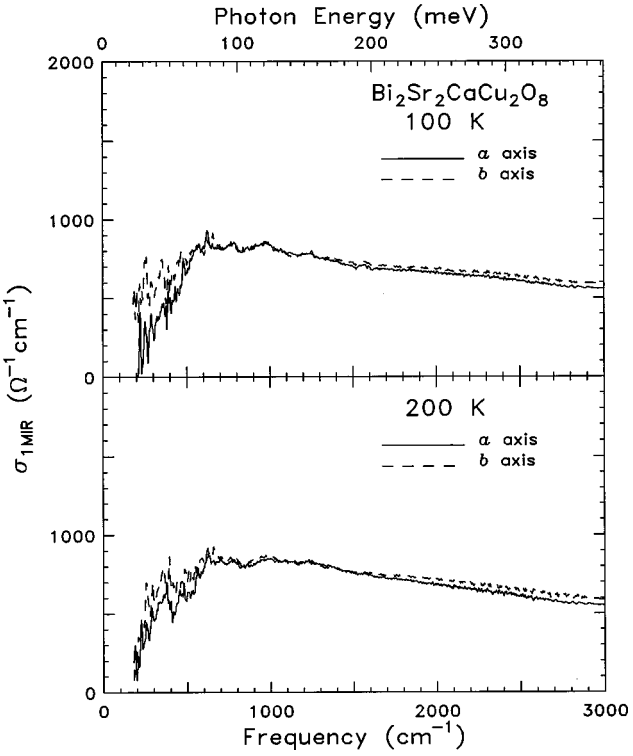

FIG. 16. Mid-infrared part of the total conductivity, comparing the *a* and *b* axes at two temperatures in the normal state.

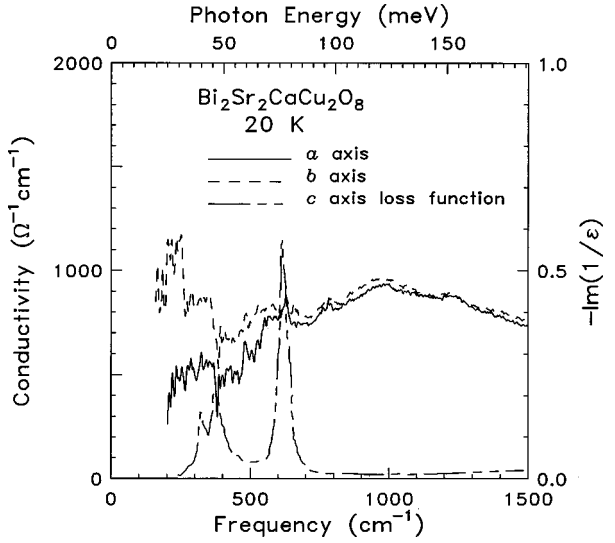

FIG. 17. Plot of $\sigma_1(\omega)$ at $T=20\,\mathrm{K}$ in the *a*- and *b*-axis polarizations along with the *c*-axis loss function, from Ref. 72.

notchlike feature, which in $YBa_2Cu_3O_{7-\delta}$ is much more evident and occurs at $\omega\sim 430\,\mathrm{cm}^{-1}$, as the superconducting energy gap. An argument against this interpretation is that the minimum in $\sigma_1(\omega)$ is also observed above T_c in nearly all samples, making its association with an energy gap very unlikely.[31,41,63]

An alternative interpretation attributes this structure to electron-phonon interactions.[44–47] As discussed by Reedyk and Timusk,[46] these interactions are between the *c*-axis longitudinal optic (LO) phonons and the *ab*-plane bound carriers. Supporting evidence for this interpretation is shown in Fig. 17, where the $Bi_2Sr_2CaCu_2O_8$ *c*-axis energy-loss function[72] (which has maxima at the LO phonon frequencies) are plotted along with *a*- and *b*-axis conductivities at 20 K. The coincidence between the loss-function maxima and $\sigma_1(\omega)$ minima is quite remarkable. Similar evidence for this effect has come from measurements on $La_2CuO_{4+\delta}$ single crystals.[60]

VII. SUPERCONDUCTING STATE

A. The superconducting condensate

We saw from the two-component analysis that the *a*-axis scattering rate for the Drude carriers is close to 150 cm^{-1} at 100 K, and that it is suddenly suppressed in the superconducting state. If this 100 K $1/\tau$ is used together with published estimates[73,74] for the Fermi velocity v_f in the CuO_2 planes to compute the mean free path l for quasiparticles propagating along this direction we obtain $l=v_f\tau\sim 100\,\text{Å}$. This number is considerably larger than the typical *ab*-plane coherence length reported[73,75] for this and other high-T_c compounds, $\xi\sim 15\,\text{Å}$. This comparison suggests that $Bi_2Sr_2CaCu_2O_8$ is in the clean limit, i.e., $l>\xi$, as was first pointed by Kamarás *et al.*[63] for $YBa_2Cu_3O_{7-\delta}$. In this limit, absorption associated with the superconducting gap is not observable because in the superconducting state most of the spectral weight moves to the zero-frequency delta function. Thus the only signature of the condensate is its inductive response, seen in the real part of the dielectric function, $\epsilon_1(\omega)$. The delta function conductivity gives, via the Kramers-Kronig relations,[76]

$$\epsilon_1(\omega)=\epsilon_{1b}-\frac{\omega_{ps}^2}{\omega^2}, \tag{15}$$

where ω_{ps} is the oscillator strength of the superconducting condensate, defined as $\omega_{ps}=4\pi n_s e^2/m$, with n_s the density of superfluid carriers. The term ϵ_{1b} is the bound-carrier contribution to $\epsilon_1(\omega)$. Hence, the condensate contribution ω_{ps} to $\epsilon_1(\omega)$ can be determined from a plot of $\epsilon_1(\omega)$ as a function of ω^{-2}. As shown in Fig. 18, this plot for the *a* axis gives a straight line whose slope is ω_{ps}^2. From this slope at $T=20\,\mathrm{K}$, we find $\omega_{ps}^a=9000\pm 200\,\mathrm{cm}^{-1}$ and $\omega_{ps}^b=8200\pm 200\,\mathrm{cm}^{-1}$. Hence, the superconducting-carrier response is larger for the *a*-axis direction.

An alternative method that obtains the same results is to estimate the missing area under $\sigma_1(\omega)$ in the superconducting state. This estimate is done by subtracting the conductivity at the lowest temperature ($T=20\,\mathrm{K}$ in this case) from the

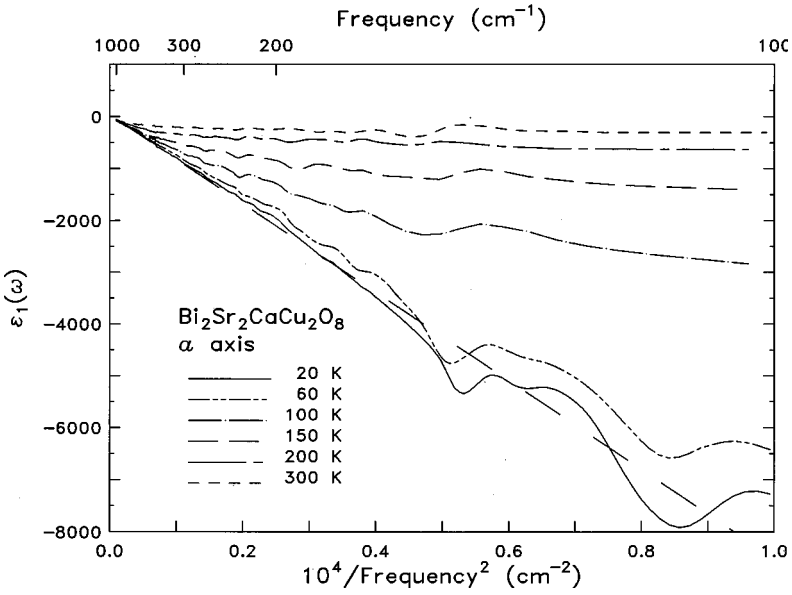

FIG. 18. ϵ_1 vs ω^{-2} in the superconducting state for the *a* direction.

conductivity just above T_c ($T=100$ K in this case). Then, the sum rule or density of superfluid carriers, $N^s_{\rm eff}m/m_b$, is evaluated by performing the integral

$$N^s_{\rm eff}(\omega)\frac{m}{m_b}\sim\int_0^{\omega}\sigma(\omega,100\,{\rm K})-\sigma(\omega,20\,{\rm K}). \qquad (16)$$

By evaluation of the integral in Eq. (16), we find $N^s_{\rm eff}m/m_b \sim 0.20$ for the *a* axis and $N^s_{\rm eff}m/m_b\sim 0.16$ for the *b* axis. Hence, by noticing that $(N_{\rm eff}m/m_b)=\omega^2_{ps}mV_{\rm cell}/4\pi e^2$ and from the known unit-cell volume of $Bi_2Sr_2CaCu_2O_8$, we find that

$$\omega^a_{\rm ps}=19\,900\sqrt{N^s_{\rm eff}}\simeq 8900\ \ {\rm cm}^{-1}$$

in the *a*-axis polarization, while $\omega^b_{ps}\simeq 8100\,{\rm cm}^{-1}$ for the *b* axis. Both quantities agree with the results from analysis of ϵ_1 described above.

B. *ab*-plane anisotropy in the London penetration depth

The London penetration length λ_L measures the distance over which an electromagnetic wave is attenuated inside a superconductor. Since this length is a measure of the superfluid response in a superconductor, it is also related to the superfluid oscillator strength ω_{ps} by $\lambda_L=c/\omega_{ps}$. In anisotropic materials, λ_L is a tensor quantity. Hence, polarized infrared spectroscopic offers a unique opportunity to determine the different components of this tensor. Other techniques, such as magnetic inductance method or muon spin resonance,[77,78] only give values of λ_L that are averages of the different components of λ_L. From the values of ω_{ps} for the *a* and *b* axes of $Bi_2Sr_2CaCu_2O_8$, we find for the London length along the *a* axis $\lambda^a_L\sim 1800$ Å, while $\lambda^b_L\sim 1960$ Å. The ratio of these two quantities is $\lambda^b_L/\lambda^a_L\sim 1.1$.

Another way to demonstrate London response of the superfluid is to calculate a generalization of the London length via

$$\lambda_L=\frac{c}{\omega\sqrt{1-\epsilon_1(\omega)}}. \qquad (17)$$

[Note that this can also be written in terms of the imaginary part of the conductivity, $\sigma_2(\omega)$, as $\lambda_L=c/\sqrt{4\pi\omega\sigma_2(\omega)}$.] Figure 19 displays λ_L for the *a* and *b* axes. The fact that both curves in Fig. 19 are nearly flat in the far infrared, approaching the values given above at $\omega=0$, suggests that the principal contribution to $\sigma_2(\omega)$ is from the superfluid carrier response, which follows $\sigma_2(\omega)\propto 1/\omega$.

There is a definite anisotropy in the penetration depth. To explain the source of this anisotropy the first thing that should be considered is whether the anisotropy that is observed in λ_L is due to mass enhancement effects. In the normal state, the *ab*-plane anisotropy in the dc resistivity, from extrapolations of the optical data and direct dc transport, is $\rho_b/\rho_a\sim 1.25$. As discussed previously, the normal-state anisotropy in the Drude plasma frequency derived from a two-component analysis of the optical data is found to be smaller than this anisotropy, i.e., $\omega^a_{pD}\ \omega^b_{pD}=1.04\pm 0.04$. Hence, most of the anisotropy in $\rho_{\rm dc}$ is due to a free-carrier relaxation rate that, at $T=100$ K, is 20% larger for the *b* axis.

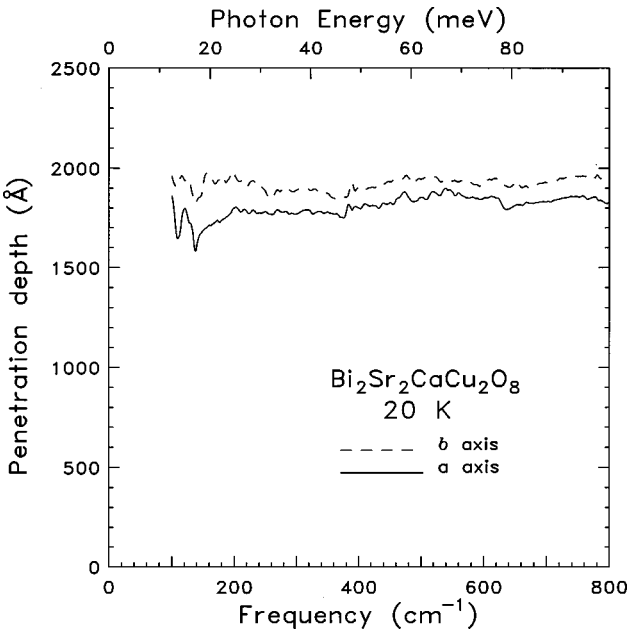

FIG. 19. London penetration length as a function of frequency using Eq. (17).

This suggests the interactions that are responsible for the relaxation of the free carriers are not isotropic but that the effective masses have a smaller anisotropy.

If we compare the superfluid plasma frequency to the Drude plasma frequency, we find for the *a* axis that ω^a_{ps} is 97% of ω^a_{pD} (essentially identical). In contrast, in the *b* direction $\omega^b_{ps}=8100\pm 200\,{\rm cm}^{-1}$ and $\omega^b_{pD}=8900\pm 200\,{\rm cm}^{-1}$, so that the superfluid plasma frequency is only about 90% of the Drude plasma frequency. We note further that the zero-temperature extrapolation of $\rho_{\rm dc}$ (or $1/\tau$) for the *b* axis appears to be finite, whereas for the *a* axis, the zero-temperature intercept is very close to zero. That the *b*-axis plasma frequency is smaller in the superconducting state suggests that the anisotropy is not related to a mass enhancement effect but instead is due to an additional (pair-breaking) scattering channel in the *b* or superlattice direction. This additional scattering causes additional absorption at finite frequencies in the superconducting state and a reduced condensate weight.

C. Optical conductivity and symmetry of the order parameter

The symmetry of the order parameter in the high-temperature superconductors has been addressed by many workers.[43,66,79–87] There is a growing consensus for an unconventional *d*-wave symmetry for this quantity. Angular-resolved photoemission spectroscopy (ARPES) has played a key role in this consensus.[43,84,85,88] In one study, Shen *et al.*[85] performed ARPES measurements on $Bi_2Sr_2CaCu_2O_8$ single crystals, finding a condensate peak that is larger and more pronounced along the Γ-*X* symmetry direction, i.e., from the center of the Brillouin zone to the *X* point in momentum space. The gap seems to vanish (within the experimental resolution of ± 2 meV) along $\langle\pi,\pi\rangle$, 45° away from the maximum-gap direction. Based on the assumption the material has tetragonal rather than orthorhombic symmetry, the authors conclude the symmetry of the order parameter is

compatible with $d_{x^2-y^2}$ symmetry pairing.[85] Recent experiments in the temperature dependence of $\lambda_L(T)$ have found a linear temperature variation that has also been interpreted has evidence of $d_{x^2-y^2}$ pairing in these materials.[66] On the other hand, this interpretation is in contradiction with other ARPES experiments performed by Kelley and co-workers.[43] These authors argue against a pure $d_{x^2-y^2}$ gap symmetry. The authors also point out that other possibilities such as mixing of *d*-wave with either *s*- or *p*-wave symmetries cannot be excluded. In spite of the controversy, one strong conclusion that can be obtained from these results is that the order parameter in the high-T_c materials appears to be highly anisotropic.

The optical conductivity can say certain things about the symmetry of the electronic structure in the superconducting state. Exactly what can be said depends on several factors: clean or dirty limit, gap symmetry, and underlying crystallographic symmetry. If the material were in the dirty limit, then the *s*-wave superconductor has a gap 2Δ in its excitation spectrum, as derived by Mattis and Bardeen.[89] The impurity scattering also has the effect of averaging any anisotropy from band-structure effects, so that the gap is reasonably isotropic, even in materials with some electronic anisotropy. At zero temperature σ_{1s} vanishes for $\omega<2\Delta$. The missing spectral weight of σ_{1s} in the range $0<\omega<2\Delta$ appears[32] in the δ function at $\omega=0$. In the case of finite temperatures, thermally exited quasiparticles can give rise to a Drude-like contribution to $\sigma_1(\omega)$ with a width in the order of $1/\tau$.

A dirty-limit superconductor with a gap function that has nodes on the Fermi surface, such as one with a *d*-wave (or *p*-wave) gap, will have finite contribution to $\sigma_1(\omega)$ for all $\omega<2\Delta_{\max}$, even at zero temperature. The reason for this is that it takes only an arbitrarily small energy to break Cooper pairs composed of electrons with momenta close to the nodes of the Fermi surface. Using a self-consistent *T*-matrix approximation, Hirschfeld *et al.*[90] carried out the calculation of σ_{1s}/σ_n for unconventional non-*s*-wave superconductors, finding a sort of pseudogap at energies below $2\Delta_{\max}$. There is a narrow Drude-like peak at low frequencies, caused by broken pairs in the nodes of the gap function.

In the clean limit, the *s*-wave superconductor retains its gap in the excitation spectrum but, as discussed above, the oscillator strength of the gap transition is small.[63] Moreover, if the scattering is largely electron-electron, the optical threshold is actually at 4Δ rather than 2Δ, because if the photon merely breaks a single Cooper pair, the drift momentum is unchanged and hence the electrical current is unaffected. Instead, two pairs must be broken, with subsequent large-angle scattering, for there to be finite $\sigma_1(\omega)$.[91] In the clean limit of the *d*-wave superconductor, with a small scattering phase shift, an expansion of σ_{1s}/σ_n in ω predicts a quadratic frequency dependence for ω close to zero in the case of a gap function with polar symmetry, whereas a ω^4 dependence occurs for a gap with axial symmetry. Hence, these results indicate that for a superconductor with anisotropic order parameter, electromagnetic radiation is always absorbed for frequencies down to $\omega=0$. However, as in the *s*-wave case, the spectral weight associated with the superconducting-state absorption is found to be small.[92]

In a polarized measurement, the *d*-wave superconductor, whether clean or dirty, has an *isotropic* response. This result can be understood as follows. Suppose the incident electric field is oriented parallel to the gap nodes, i.e., in the 45° direction. This field always can be decomposed into components along the *a* and *b* directions, which are the directions of the gap minima. Similarly, a field that is oriented along a direction where the gap is maximum may be constructed from components parallel to the nodes. Because the magnitude of the gap function has fourfold symmetry whereas the *ab*-plane conductivity tensor has at most twofold (dipolar) symmetry, the gap anisotropy does not contribute to a conductivity anisotropy.

Finally, in an orthorhombic crystal, the dielectric tensor has three different components, with principal axes along the *a, b,* and *c* crystallographic directions. Unlike the tetragonal symmetry case, the orthorhombic crystal cannot have a pure *d*-wave gap, although $d+s$ is allowed.[93]

Our results unambiguously show that the *ab*-plane optical response of $Bi_2Sr_2CaCu_2O_8$ is anisotropic both above and below T_c. As illustrated in Figs. 2 and 3, the *a*-axis reflectance in the superconducting state reaches almost 100% for frequencies in the far infrared, whereas there is a difference in the reflectance level ($\mathcal{R}_a>\mathcal{R}_b$) on the order 1–2 %. A Kramers-Kronig analysis of the reflectance for the two polarizations gives anisotropy in $\sigma_1(\omega)$. In the normal state, the far-infrared conductivity is about 20% larger for polarization along the *a* axis. In the superconducting state, $\sigma_1(\omega)$ is a factor of 2 larger for the *b* axis below 300 cm^{-1} and down to the lowest frequency measured in the experiment. Finally, the penetration depth is about 10% larger for the *a*-axis direction.

If a one-component analysis with a frequency-dependent $1/\tau$ is used to explain these results, the superconducting-state conductivity must then be due to excitations across the superconducting gap. The observed anisotropy in $\sigma_1(\omega)$ below T_c implies an order parameter consistent with a C_{2v} rather than a C_{4v} symmetry. If this interpretation is taken, these data are incompatible with *s*-wave pairing or with a pure $d_{x^2-y^2}$ gap symmetry. The results would be compatible with a combination of *s* and *d* pairing.[43]

If the conductivity is decomposed into two components, the observed anisotropy of the *ab*-plane conductivity could be due to two factors. Above T_c the free-carrier damping rate is 20% stronger along *b* [$1/\tau(100\,\mathrm{K})=180\,\mathrm{cm}^{-1}$ for the *b* axis and 150 cm^{-1} for the *a* axis]. Above and below T_c, the mid-infrared component has a larger contribution along *b* than along the *a* axis. This anisotropy is compatible with the observed orthorhombic unit cell in this material.

VIII. CONCLUSIONS

In conclusion, the anisotropy of the *ab*-plane of the copper-oxide superconductors has been studied by measuring the polarized reflectance of single-domain crystals of $Bi_2Sr_2CaCu_2O_8$. There is significant *ab*-plane anisotropy in the optical properties of this material. In the normal state, the infrared conductivity is about 20% higher along the *a* axis than the *b* axis. A similar *ab*-plane anisotropy is observed in the normal-state dc resistivity of similar samples.

The normal-state *ab*-plane conductivity exhibits non-Drude behavior, characterized by strong temperature depen-

dence in the far infrared and a much weaker temperature variation in the mid-infrared region. If the conductivity is analyzed in the framework of a two-component picture, the low-frequency part can be regarded as Drude-like in nature, with a scattering rate that is linear in temperature. This behavior is consistent with the linear temperature dependence of the dc resistivity. The coupling constant obtained in this analysis is $\lambda \sim 0.3-0.4$ in all samples.

The *ab*-plane anisotropy observed in the normal-state conductivity of these samples persists in the superconducting state as well. The optical conductivity at low frequencies is a factor of 2 larger along the *b* axis than along the *a* axis. This suggests that either an anisotropic order parameter with a twofold symmetry (C_{2v}) rather than a fourfold symmetry (C_{4v}) or that the mid-infrared component of the optical conductivity is anisotropic.

Finally, estimates of the London penetration lengths display anisotropy, with $\lambda_b/\lambda_a \sim 1.1$. This result suggests some additional elastic scattering mechanism in the *b* axis of the crystal is giving rise to some kind of pair-breaking effect that is causing λ_L to be larger along this direction ($\lambda_L^b \sim 2000$ Å compared to $\lambda_L^a \sim 1800$ Å).

ACKNOWLEDGMENTS

We would like to acknowledge many discussions with P.J. Hirschfeld. Work at Florida was supported by the NSF—Solid State Physics—through Grant No. DMR-9705108. Work at Wisconsin was supported by the DOE.

*Present address: NASA/GODDARD, MS 551, Bldg. 5, Rm. C38, Greenbelt, MD 20771.

[1] D. B. Tanner and T. Timusk, in *Physical Properties of High Temperature Superconductors III*, edited by D. M. Ginsberg (World Scientific, Singapore, 1992), p. 363.

[2] B. Koch, H. P. Geserich, and T. Wolf, Solid State Commun. **71**, 495 (1989).

[3] Z. Schlesinger, R. T. Collins, F. Holtzberg, C. Field, S. H. Blanton, U. Welp, G. W. Crabtree, Y. Fang, and J. Z. Liu, Phys. Rev. Lett. **65**, 801 (1990).

[4] T. Pham, M. W. Lee, H. D. Drew, U. Welp, and Y. Fang, Phys. Rev. B **44**, 5377 (1991).

[5] H. P. Geserich, B. Koch, M. Dürrler, and Th. Wolf, in *Electronic Properties of High-T_c Superconductors and Related Compounds*, edited by H. Kuzmany, M. Mehring, and J. Fink, Springer Series in Solid-State Sciences Vol. 99 (Springer-Verlag, Berlin, 1990), p. 290.

[6] J. Schützmann, B. Gorshunov, K. F. Renk, J. Münzel, A. Zibold, H. P. Geserich, A. Erb, and G. Müller-Vogt, Phys. Rev. B **46**, 512 (1992).

[7] L. D. Rotter, Z. Schlesinger, R. T. Collins, F. Holtzberg, C. Field, U. W. Welp, G. W. Crabtree, J. Z. Liu, Y. Fang, K. G. Vandervoort, and S. Fleshler, Phys. Rev. Lett. **67**, 2741 (1991).

[8] S. L. Cooper, A. L. Kotz, M. A. Karlow, M. V. Klein, W. C. Lee, J. Giapintzakis, and D. M. Ginsberg, Phys. Rev. B **45**, 2549 (1992).

[9] D. N. Basov, R. Liang, D. A. Bonn, W. N. Hardy, B. Dabrowski, M. Quijada, D. B. Tanner, J. P. Rice, D. M. Ginsberg, and T. Timusk, Phys. Rev. Lett. **74**, 598 (1995).

[10] T. A. Friedmann, M. W. Rabin, J. Giapintzakis, J. P. Rice, and D. M. Ginsberg, Phys. Rev. B **42**, 6217 (1990).

[11] S. A. Sunshine, T. Siegrist, L. F. Schneemeyer, D. W. Murphy, R. J. Cava, B. Batlogg, R. B. van Dover, R. M. Fleming, S. H. Glarum, S. Nakahara, R. Farrow, J. J. Krajewski, S. M. Zahurak, J. V. Waszczak, J. H. Marshall, P. Marsh, L. W. Rupp, Jr., and W. F. Peck, Phys. Rev. B **38**, 893 (1988).

[12] T. M. Shaw, S. A. Shivashsnkar, S. J. La Placa, J. J. Cuomo, T. R. McGuire, R. A. Roy, K. H. Kelleher, and D. S. Yee, Phys. Rev. B **37**, 9856 (1988).

[13] E. A. Hewat, J. J. Capponi, and M. Marezio, Physica C **157**, 502 (1989).

[14] M. A. Quijada, D. B. Tanner, R. J. Kelley, and M. Onellion, Physica C **235-240**, 1123 (1994).

[15] M. A. Quijada, Ph.D. thesis, University of Florida, 1994.

[16] M. Reedyk, D. A. Bonn, J. D. Garrett, J. E. Greedan, C. V. Stager, T. Timusk, K. Kamarás, and D. B. Tanner, Phys. Rev. B **38**, 11 981 (1988).

[17] K. Kamarás, S. L. Herr, J. S. Kim, G. R. Stewart, D. B. Tanner, and T. Timusk, in *Electronic Properties of High-T_c Superconductors and Related Compounds* (Ref. 5), p. 260.

[18] Yun-Yu Wang, Goufu Feng, and A. L. Ritter, Phys. Rev. B **42**, 420 (1990).

[19] J. H. Kim, I. Bozovic, J. S. Harris, Jr., W. Y. Lee, C.-B. Eom, and T. H. Geballe (unpublished).

[20] O. V. Kosogov, M. V. Belousov, V. A. Vasil'ev, V. Y. Davydov, K. G. Dyo, A. A. Kopylov, V. D. Petrikov, and V. V. Tret'yakov, Pis'ma Zh. Eksp. Teor. Fiz. **48**, 488 (1989) [JETP Lett. **48**, 530 (1989)].

[21] J. Humlíček, E. Schmidt, L. Boûánek, M. Garriga, and M. Cardona, Solid State Commun. **73**, 127 (1990).

[22] A. M. Rao, P. C. Eklund, G. W. Lehman, D. W. Face, G. L. Doll, G. Dresselhaus, and M. S. Dresselhaus, Phys. Rev. B **42**, 193 (1990).

[23] P. Calvani, M. Capizzi, S. Lupi, P. Maselli, D. Peschiaroli, and H. Katayama-Yoshida, Solid State Commun. **74**, 1333 (1990).

[24] M. A. Quijada, D. B. Tanner, R. J. Kelley, and M. Onellion, Z. Phys. B: Condens. Matter **94**, 255 (1994).

[25] A. Puchkov, P. Fournier, D. N. Basov, T. Timusk, A. Kapitulnik, and N. N. Kolesnikov, Phys. Rev. Lett. **77**, 3212 (1996).

[26] D. N. Basov, R. Liang, B. Dabrowski, D. A. Bonn, W. N. Hardy, and T. Timusk, Phys. Rev. Lett. **77**, 4090 (1996).

[27] A. V. Puchkov, D. N. Basov, and T. Timusk, J. Phys.: Condens. Matter **8**, 10 049 (1996).

[28] H. L. Liu, M. A. Quijada, D. B. Tanner, H. Berger, G. Margaritondo, R. J. Kelley, and M. A. Onellion, Eur. Phys. J. B **8**, 47 (1999).

[29] H. L. Liu, M. A. Quijada, A. Zibold, Y.-D. Yoon, D. B. Tanner, G. Cao, J. E. Crow, H. Berger, G. Margaritondo, L. Forr, Beom-Hoan O, J. T. Markert, R. J. Kelly, and M. Onellion, J. Phys.: Condens. Matter **11**, 239 (1999).

[30] L. Forro, G. L. Carr, G. P. Williams, D. Mandrus, and L. Mihaly, Phys. Rev. Lett. **65**, 1941 (1990).

[31] D. B. Romero, G. L. Carr, D. B. Tanner, L. Forro, D. Mandrus, L. Mihály, and G. P. Williams, Phys. Rev. B **44**, 2818 (1991).

[32] R. E. Glover and M. Tinkham, Phys. Rev. **107**, 844 (1956); **108**, 1175 (1957).

[33] D. B. Tanner, D. B. Romero, K. Kamarás, G. L. Carr, L. Forro, D. Mandrus, L. Mihály, and G. P. Williams, in *Electronic Structure and Mechanisms for High-Temperature Superconductivity*, edited by G. C. Vezolli *et al.* (Plenum, New York, 1991).
[34] D. B. Romero, C. D. Porter, D. B. Tanner, L. Forro, D. Mandrus, L. Mihaly, G. L. Carr, and G. P. Williams, Solid State Commun. **82**, 183 (1992).
[35] D. B. Romero, C. D. Porter, D. B. Tanner, L. Forro, D. Mandrus, L. Mihaly, G. L. Carr, and G. P. Williams, Phys. Rev. Lett. **68**, 1590 (1992).
[36] P. D. Han and D. A. Payne, J. Cryst. Growth **104**, 201 (1990).
[37] Frederick Wooten, *Optical Properties of Solids* (Academic, New York, 1972).
[38] M. K. Kelly, P. Barboux, J.-M. Tarascon, D. E. Aspnes, P. A. Morris, and W. A. Bonner, Physica C **162-164**, 1123 (1989).
[39] J. W. Allen and J. C. Mikkelsen, Phys. Rev. B **15**, 2952 (1977).
[40] I. Bozovic, K. Char, S. J. B. Yoo, A. Kapitulnik, M. R. Beasley, T. H. Geballe, Z. Z. Wang, S. Hagen, N. P. Ong, D. E. Aspnes, and M. K. Kelly, Phys. Rev. B **38**, 5077 (1988).
[41] F. Gao, D. B. Romero, D. B. Tanner, J. Talvacchio, and M. G. Forrester, Phys. Rev. B **47**, 1036 (1993).
[42] Y. Hwu, L. Lozzi, M. Marsi, S. La Rosa, M. Winokur, P. Davis, M. Onellion, H. Berger, F. Gozzo, F. Lévy, and G. Margaritondo, Phys. Rev. Lett. **67**, 2573 (1991).
[43] R. J. Kelley, Jian Ma, G. Margaritondo, and M. Onellion, Phys. Rev. Lett. **71**, 4051 (1993).
[44] T. Timusk, C. D. Porter, and D. B. Tanner, Phys. Rev. Lett. **66**, 663 (1991).
[45] T. Timusk and D. B. Tanner, Physica C **169**, 425 (1990).
[46] M. Reedyk and T. Timusk, Phys. Rev. Lett. **69**, 2705 (1992).
[47] M. Reedyk, Ph.D. thesis, McMaster University, 1992.
[48] C. M. Varma, P. B. Littlewood, S. Schmitt-Rink, E. Abrahams, and A. E. Ruckenstein, Phys. Rev. Lett. **63**, 1996 (1989).
[49] P. B. Littlewood and C. M. Varma, J. Appl. Phys. **69**, 4979 (1991).
[50] A. Virosztek and J. Ruvalds, Phys. Rev. B **42**, 4064 (1990).
[51] P. W. Anderson, Science **235**, 1196 (1987); in *Frontiers and Borderlines in Many Particle Physics*, edited by J. R. Schrieffer and R. A. Broglia (North-Holland, Amsterdam, 1989); Phys. Rev. Lett. **64**, 1839 (1990); Science **256**, 1526 (1992).
[52] V. J. Emery, S. A. Kivelson, and H. Q. Lin, Phys. Rev. Lett. **64**, 475 (1990); V. J. Emery and S. A. Kivelson, Physica C **209**, 597 (1993).
[53] P. Monthoux and D. Pines, Phys. Rev. B **49**, 4261 (1994).
[54] T. Holstein, Phys. Rev. **96**, 535 (1954); Ann. Phys. (N.Y.) **29**, 410 (1964).
[55] S. Uchida, T. Ido, H. Takagi, T. Arima, Y. Tokura, and S. Tajima, Phys. Rev. B **43**, 7942 (1991).
[56] G. A. Thomas, in *Proceedings of the Thirty-Ninth Scottish Universities Summer School in Physics*, edited by D. P. Tunstall and W. Barford (Hilger, Bristol, 1991), p. 196.
[57] S. L. Cooper, D. Reznik, A. Kotz, M. A. Karlow, R. Liu, M. V. Klein, W. C. Lee, J. Giapintzakis, D. M. Ginsberg, B. Veal, and A. P. Paulikas, Phys. Rev. B **47**, 8233 (1993).
[58] Y. Tokura, H. Takagi, T. Arima, S. Koshihara, T. Ido, S. Ishibashi, and S. Uchida, Physica C **162-164**, 1231 (1989).
[59] S. Lupi, P. Calvani, M. Capizzi, P. Maselli, W. Sadowski, and E. Walker, Phys. Rev. B **45**, 12 470 (1992).
[60] M. A. Quijada, D. B. Tanner, F. C. Chou, D. C. Johnston, and S-W. Cheong, Phys. Rev. B **52**, 15 485 (1995).
[61] G. A. Thomas, M. Capizzi, J. Orenstein, D. H. Rapkine, A. J. Millis, P. Gammel, L. F. Schneemeyer, and J. V. Waszczak, in *Proceedings of the International Symposium on Electronic Structure of High T_c Superconductors*, edited by A. Bianconi (Pergamon, Oxford, 1988), p. 169.
[62] J. Orenstein, G. A. Thomas, A. J. Millis, S. L. Cooper, D. H. Rapkine, T. Timusk, L. F. Schneemeyer, and J. V. Waszczak, Phys. Rev. B **42**, 6342 (1990).
[63] K. Kamarás, S. L. Herr, C. D. Porter, N. Tache, D. B. Tanner, S. Etemad, T. Venkatesan, E. Chase, A. Inam, X. D. Wu, M. S. Hegde, and B. Dutta, Phys. Rev. Lett. **64**, 84 (1990).
[64] P. B. Allen, T. B. Beaulac, F. S. Khan, W. H. Butler, F. J. Pinski, and J. H. Swihart, Phys. Rev. B **34**, 4331 (1986).
[65] F. Gao, G. L. Carr, C. D. Porter, D. B. Tanner, G. P. Williams, C. J. Hirschmugl, B. Dutta, X. D. Wu, and S. Etemad, Phys. Rev. B **54**, 700 (1996).
[66] W. N. Hardy, D. A. Bonn, D. C. Morgan, Ruixing Liang, and Kuan Zhang, Phys. Rev. B **70**, 3999 (1993).
[67] J. M. Chwalek, C. Uher, J. F. Whitaker, G. A. Mourou, J. Agostinelli, and M. Lelental, Appl. Phys. Lett. **57**, 1696 (1990).
[68] E. J. Nicol and J. P. Carbotte, Phys. Rev. B **44**, 7741 (1991).
[69] F. A. Miranda, W. L. Gordon, K. B. Bhasin, V. O. Heinen, and J. D. Warner, J. Appl. Phys. **70**, 5450 (1991).
[70] M. C. Nuss, P. M. Mankiewich, M. L. O'Malley, E. H. Westerwick, and P. B. Littlewood, Phys. Rev. Lett. **66**, 3305 (1991).
[71] K. Holczer, L. Forro, L. Mihaly, and G. Gruner, Phys. Rev. Lett. **67**, 152 (1991).
[72] A. Zibold, M. Dürrler, A. Gaymann, H. P. Geserich, N. Nucker, V. M. Burlakov, and P. Müller, Physica C **193**, 171 (1992).
[73] S. A. Wolf and V. Z. Kresin, IEEE Trans. Magn. **27**, 852 (1991).
[74] P. B. Allen, W. E. Pickett, and H. Krakauer, Phys. Rev. B **36**, 3926 (1987).
[75] A. Umezawa, G. W. Crabtree, J. Z. Liu, T. J. Moran, S. K. Malik, L. H. Nunez, W. L. Kwok, and C. H. Sowers, Phys. Rev. B **38**, 2843 (1988).
[76] T. Timusk and D. B. Tanner, in *Physical Properties of High Temperature Superconductors I*, edited by D. M. Ginsberg (World Scientific, Singapore, 1989), p. 339.
[77] J. R. Cooper, L. Forró, and B. Keszei, Nature (London) **343**, 444 (1990).
[78] Y. Tanaka, M. Fukutomi, and T. Asano, Jpn. J. Appl. Phys., Part 2 **27**, L209 (1988).
[79] A. T. Fiory, A. F. Hebard, P. M. Mankiewich, and R. E. Howard, Phys. Rev. Lett. **61**, 1419 (1988).
[80] D. A. Bonn, R. Liang, T. M. Riseman, D. J. Baar, D. C. Morgan, K. Zhang, P. Dosanjh, T. L. Duty, A. MacFarlane, G. D. Morris, J. H. Brewer, W. N. Hardy, C. Kallin, and A. J. Berlinsky, Phys. Rev. B **47**, 11 314 (1993).
[81] J. F. Annet, N. Goldenfeld, and S. R. Renn, Phys. Rev. B **43**, 2778 (1991).
[82] J. F. Annet and N. Goldenfeld, J. Low Temp. Phys. **89**, 197 (1992).
[83] Z. Ma, R. C. Taber, L. W. Lombardo, A. Kapitulnik, M. R. Beasley, P. Merchant, C. B. Eom, S. Y. Hou, and J. M. Phillips, Phys. Rev. Lett. **71**, 781 (1993).
[84] D. S. Dessau, Ph.D. dissertation, Stanford University, 1992.
[85] Z.-X. Shen, D. S. Dessau, B. O. Wells, D. M. King, W. E. Spicer, A. J. Arko, D. Marshall, L. W. Lombardo, A. Kapitulnik, P. Dickinson, S. Doniach, J. DiCarlo, A. G. Loeser, and C. H. Park, Phys. Rev. Lett. **70**, 1553 (1993).
[86] D. J. Van Harlingen, Rev. Mod. Phys. **67**, 515 (1995).
[87] J. P. Kirtley, C. C. Tsuei, M. Rupp, J. Z. Sun, L. S. Yu-Jahnes, A.

Gupta, M. B. Ketchen, K. A. Moler, and M. Bhushan, Phys. Rev. Lett. **76**, 1336 (1996).
[88] D. Hong, J. C. Campuzano, K. Gofron, C. Gu, R. Liu, B. W. Veal, and G. Jennings, Phys. Rev. B **50**, 1333 (1994).
[89] D. C. Mattis and J. Bardeen, Phys. Rev. **111**, 412 (1958).
[90] P. J. Hirschfeld, P. Wölfle, J. A. Sauls, D. Einzel, and W. O. Putikka, Phys. Rev. B **40**, 6695 (1989).
[91] J. Orenstein, S. Schmitt-Rink, and A. E. Ruckenstein, in *Electronic Properties of High-T_c Superconductors and Related Compounds* (Ref. 5).
[92] S. M. Quinlan, P. J. Hirschfeld, and D. J. Scalapino, Phys. Rev. B **53**, 8575 (1996).
[93] Q. P. Li, B. E. C. Koltenbah, and Robert Joynt, Phys. Rev. B **48**, 437 (1993).